Metastable defects in hydrogenated amorphous silicon

Richard S. Crandall
RCA Laboratories, David Sarnoff Research Center, P.O. Box 432, Princeton, New Jersey 08543-0432
(Received 12 May 1986; revised manuscript received 20 November 1986)

Measurements of the properties of metastable defects in hydrogenated amorphous silicon are presented. The emission energy and time are found with use of deep-level transient spectroscopy. In some cases the metastable states can be associated with specific impurities. The use of transient capacitance and photovoltaic measurements to study light- and current-induced defects in hydrogenated amorphous silicon, *a*-Si:H, is described in detail for *p-i-n* and *n-i-p* solar-cell structures. The sign and annealing energy of defects in the *i* layer are found. The sign of the defect correlates with the injected charge. Both positive and negative charged defects are produced by uniformly absorbed illumination or double injection. The positively charged defect can be identified with the Staebler-Wronski effect. Both defects cause solar-cell degradation. The activation energy for annealing the negatively charged defect is about 1 eV for most samples. Some samples have a distribution of activation energies. The hole-trap defect has an activation energy higher than 1.4 eV. The defect-production rate is thermally activated with an activation energy slightly higher than the annealing energy. It is argued that the defects are positively and negatively charged dangling bonds, thermally produced when a charge is injected at a band edge.

I. INTRODUCTION

There is considerable interest in metastable defects (MSD's) in amorphous materials. These states can be formed by radiation and subsequently removed by annealing at moderate temperatures. Because the first evidence for these states in *a*-Si:H was obtained by Staebler and Wronski,[1] metastable changes in the properties of *a*-Si:H are referred to as the Staebler-Wronski, SW, effect. Although there is much scientific interest in the SW effect, a principle concern at present is the degradation of solar cells. Despite the remaining questions as to the exact mechanism, there is no doubt that it is related to the SW effect.

Intense investigation of metastable effects began after the observation[1] that both photoconductivity and dark conductivity decreased following irradiation of *a*-Si:H at room temperature. The effect could be removed by annealing the film above about 150 °C. Additional metastable changes have been observed in electrical conductivity,[1,2] photoconductivity,[2,3] luminescence,[4,5] electron paramagnetic resonance,[6–8] gap state density,[9–13] subband-gap optical absorption,[13] and solar-cell properties.[14–19] These metastable effects can be produced by current flow in the film as well as light.[14–17] It seems clear that all the metastable effects in *a*-Si:H are intimately related. Various measurements[2,15–17,20] of the annealing rate have shown that the activation energies, E_e, for this process fall into three groupings: 0.4, 1, and 1.5 eV.

The MSD formed in *a*-Si:H possess varied and perhaps unique properties. First, the defect is usually stable below about 100 °C. If the annealing follows simple escape kinetics, this means that the activation energy must be around 1 eV. This limits the mechanism to weak bond breaking, thermal emission from a state below midgap, or escape over a high potential barrier. Deep-level transient spectroscopy (DLTS) measurements show that the defects can trap either an electron or hole.[15,20] It does not appear to be possible to determine whether the defect is created during the degradation process or merely captures a free carrier from a band edge.

Although MSD can be found in a large variety of *a*-Si:H samples, there does not appear to be a significant correlation with sample preparation. There is mixed evidence regarding doping. Some find no effect with doping while others do. In two instances the defect density and properties could be correlated with oxygen[15] and carbon.[17] However, to significantly increase the density of defects requires nearly percent impurity concentrations. Also, the defects associated with carbon are different from those associated with oxygen.

A characteristic feature of the SW effect, not universally appreciated, is that the production of the MSD is thermally activated. This is the main reason why the cross section for defect formation is so low at room temperature. What is peculiar or remarkable is that the activation energy, E_p, for the defect production is nearly equal to the activation energy, for annealing.[15] The energies differ by as little as 10% with $E_p > E_e$. This relationship holds over a wide range of activation energies; from as low as 0.35 eV to nearly 1.8 eV.

This paper presents a systematic study of the MSD's encountered in various solar-cell device structures. The principle spectroscopic tool used is a variation of the familiar DLTS (Ref. 21) method. The major innovation to the usual application of DLTS is to carry out the measurements near the annealing temperature for the MSD to study the defect itself rather than the consequences of the defect. The defect properties, such as energy level and density, can conveniently be determined by measuring the recovery of the photocurrent, capacitance, and photovoltage following disturbances produced by charge changes

in the defect. One can momentarily stress the sample to form the defect, then monitor recovery from the stress. This allows the powerful DLTS techniques of signal averaging and data analysis to be applied.

Section II outlines the measurement and data-analysis methods with particular emphasis on changes in DLTS needed to measure MSD. Because capacitance measurements are made on a variety of device structures, Sec. III gives a detailed discussion of measurement and analysis of steady-state capacitance of Schottky-barrier and *p-i-n* devices. Section IV points out the modifications of the interpretation of transient capacitance measurement required for *p-i-n* devices. Section V gives data for solar-cell degradation while Sec. VI presents the results for the annealing of the degradation. Finally the results are discussed in light of various models and summarized in the last two sections.

II. MEASUREMENT PROCEDURE

A. Data production and analysis

Either a light flash or a forward bias current pulse can be used to degrade a solar cell and thus form or populate the MSD. The time sequence of a typical measurement is shown in Fig. 1. The sample is reverse biased until a steady state is reached. Then a short forward bias voltage pulse or light flash of duration t_p is used to form electron-hole pairs that can be captured by the defects. After the pulse, the system relaxes to its steady-state value as electrons or holes, thermally emitted from the defects, are removed from the sample by transport. Except for the fortuitous case where electrons and holes are trapped in equal numbers and the emission rates are the same, the capacitance will be changed by the degradation pulse. Usually one sign of carrier is predominantly trapped. The sign and magnitude of the initial capacitance change is related to the nature and amount of trapped charge. The shape of the decay transient gives information about the energy level of the trapped charge. Usually the capacitance relaxes exponentially with a single characteristic time constant, τ. Because the system returns to the steady state by thermal emission, τ is a strong function of temperature. Most of the MSD's have a large emission energy, around 1 eV. Measurements must be carried out at temperatures considerably above room temperature. Otherwise, the decay time would be many hours. This feature distinguishes these measurements from the usual DLTS measurements.

Changes in both solar-cell properties and capacitance can be observed, following degradation. The photocurrent, the dark current, and the photovoltage all relax to their original values following degradation. These quantities do not give the sign of the trapped charge, but they are relatively easy to measure. It is sometimes possible to correlate their changes with capacitance changes and determine the sign of the trapped charge.

The analysis of the decay transient depicted in Fig. 1 proceeds in the usual manner.[21,22] The measured quantity is the DLTS function, $S(t)$. For capacitance transients, $S(t)$ is the difference in the capacitance, $C(t)$, at two different times t_2 and t_1. Thus

$$S(t)=C(t_2)-C(t_1)\ . \tag{1}$$

The time difference, t_2-t_1, is referred to as the time window. If $S(t)$ is to have a rigorous physical basis, then the time window should be chosen according to the following relationships:

$$t_2-t_1=c\bar{t}\ , \tag{2}$$

$$\bar{t}=(t_2+t_1)/2\ , \tag{3}$$

where c is an arbitrary constant dictated by the constraints of the experiment. In this case $S(t)$ is proportional to the energy response function which, for capacitance transients, is a measure of the density of states per unit energy, $N(E)$.

If the MSD has a single energy level or the levels are well separated in energy then the decay transient will be a single exponential. An example for $\tau=10$ s is shown in Fig. 2, where $C(t)$ and $S(t)$ are plotted versus $\ln(\bar{t})$. For this figure the constant c is 0.2292 so that there are ten equally spaced points per decade. $S(t)$ shows a distinctive peak at a time that is close to the characteristic emission time, τ, for the state. The values were calculated, assuming the depletion width approximation applies, for an *n*-type Schottky-barrier device.

The emission time and emission energy, E_e, are related by

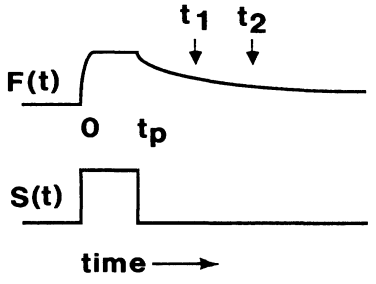

FIG. 1. Typical experimental timing sequence for measurement of the recovery from stress following device degradation. $F(t)$ is any parameter that is changed by stress and S the stress.

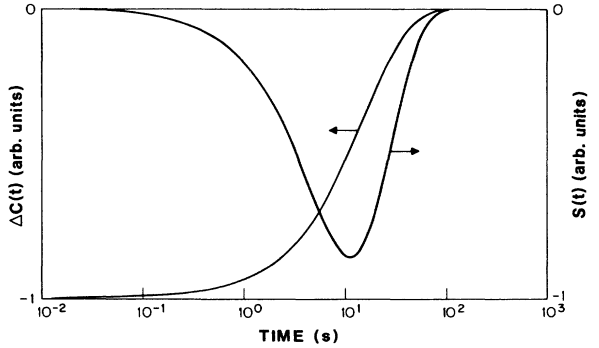

FIG. 2. Calculated capacitance change vs the logarithm of the time. There is a single energy level with $\tau=10$ s. $S(t)$ derived from $\Delta C(t)$.

$$E_e = kT \ln(\nu\tau) , \quad (4)$$

where k is Boltzmann's constant, T the absolute temperature, and ν the attempt-to-escape frequency. To find E_e and ν it is necessary to measure $S(t)$ at a variety of temperatures and plot $\ln(\tau)$ versus $1/T$. Usually this plot yields a straight line whose slope is E_e. The intercept gives ν.

The above discussion referred to an analysis of a decay transient at a fixed temperature. In the usual DLTS method, t_1 and t_2 are fixed and the temperature is varied over a wide range to construct the DLTS function. Because of the high-activation energy for charge capture and emission[15] of the defects involved in this study the times involved are usually longer than seconds. In this case the standard low-temperature DLTS techniques are not practical. Since we use information from the entire decay transient, the complete DLTS function can be constructed at a fixed temperature. This method does not give any additional information over the usual approach, but is easier to use when the decay times are long.

In some cases charges of both sign are trapped so that the decay transient is no longer a pure exponential. Nevertheless, if the decay times are well separated in energy, the DLTS function can still be used to find the emission energy for the two trap states. An example of the decay transient and $S(t)$ for both a hole and an electron trap is given in Fig. 3. At short times there is an excess of trapped electrons so that the capacitance change is negative. At longer times all the electrons have been emitted from the defects leaving an excess of holes and thus an increase in the capacitance. The emission energy for both signs of charge can be clearly determined from $S(t)$ shown in Fig. 3. Furthermore, since these peak positions move at different rates as the temperature changes they can be more easily resolved by changing the temperature.

Even though the above analysis was outlined for a capacitance transient, it applies equally well to the transient changes in solar-cell properties such as photovoltage or photocurrent.

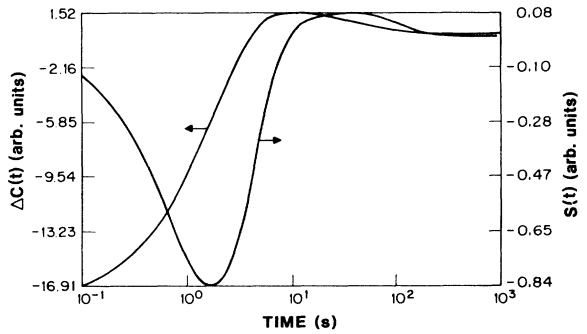

FIG. 3. Calculated change in capacitance for the case where both electrons and holes are trapped at different energies. A negative capacitance change indicates an excess of trapped electrons and a positive capacitance change an excess of trapped holes.

B. Experimental details

The samples were fabricated by dc glow-discharge decomposition of high-purity silane using various dopants. Since the details of the solar-cell production at RCA have been outlined in various publications,[23] we shall only give details if they affect the results under discussion.

Various device structures were used depending on the material to be investigated. The most commonly available structures were solar-cell quality p-i-n on n-i-p devices. The convention is that the light enters through the p layer in a p-i-n device and through the n layer in an n-i-p device. Schottky barriers and p-n junctions were also used. The p-i-n structures were glass/conducting transparent oxide/p-i-n/metal. The n-i-p structures were conducting transparent oxide/n-i-p/metal. These latter two structures are well suited for study of the intrinsic layer. The p-type and n-type doping was by means of diborane or phosphine from the gas phase. The devices used in this study were optimized solar cells containing about 1% by volume of boron and phosphorous in the p and n layers, respectively. The i layer was undoped, unless noted. The thickness of the i layer, unless otherwise noted, was between 0.5 and 0.6 μm.

To study the n layer, 1–4-μm-thick Schottky-barrier cells were fabricated on stainless steel using Pt for the blocking contact. Stainless steel makes a fairly good Ohmic contact to a-Si:H. To insure good Ohmic contact, a thin heavily doped n^+ layer was deposited before the n layer. When the thick layer is lightly doped or intrinsic, gas used to dope the n layer is thoroughly purged from the system before deposition of the final layer.

To study the p layer, 0.5-μm-thick boron doped a-Si:H:C alloy layers were grown on glass substrates, coated with indium-tin oxide or other transparent conducting material. A thin, heavily n-type layer completed the p-n junction contacts to the n^+ layer. To make an ideal p-n junction one requires an Ohmic contact to the p layer. In all our attempts, we were not able to make an Ohmic contact to the p layer. This does not preclude measurements and in some instances is an advantage because there are two junctions in the sample. One at the p-n interface and the other at the p indium-tin oxide interface, both of which can be studied separately.

The sample numbering convention used in this article is that the letters refer to sample type, i.e., pin means p-i-n, nip means n-i-p, Shn means n-type Schottky barrier, and pn means p-n-junction device.

The a-Si:H solar-cell devices were mounted on a hot stage in the center of a large can filled with an inert gas. The heater of the stage and a platinum resistor were used in components of a negative feedback system to hold the temperature of the stage constant. The temperature of the sample was measured using a thermocouple.

The temperature was set, voltage applied to the cell, and current or capacitance measured using an Apple II computer and associated peripherals. Sample voltage was derived from a programmable power supply. This, in turn, was controlled by a fast 12-bit digital-to-analog (DA) converter permitting voltage pulses to be applied to the sample. Capacitance or conductance were measured

with a Hayes Associates programmable phase-sensitive detector. Its output was measured using a 12-bit analog-to-digital (AD) converter capable of 50 μs time resolution. The DA and AD were made by Interactive Microware.

The use of a computer to control the experiment is necessary because of the large amount of data that must be processed for a single transient. The current or capacitance transients are followed typically over five decades in time and the entire transient is recorded using multiple time windows. The main reason for using this approach instead of the normal method of scanning the temperature using a fixed time window is that the long times involved for the transients in the present experiments makes scanning the temperature impractical. The scan rate must be much slower than the inverse of the decay time.

Photocurrent and photovoltage were measured, using the same system, with the 12-bit (binary digit) AD used to measure the photovoltage or current. The light source was either a krypton laser, giving wavelengths throughout the visible, or a xenon arc and appropriate filters.

Because only one capacitance, voltage or current transient is taken it is imperative to minimize the noise in the system. Signal averaging to reduce noise is not practical for transients of 100 s or longer. The noise is not so important for the transients themselves but for the function $S(t)$ which is obtained from the derivative of the transient. This problem is most serious at long times when the signals are smallest. Fortunately, at longer times one does not require points spaced so closely in time. Thus it is possible to treat the data with a digital filter whose pass band frequency decreases with time. Time resolution is not so important at long times because the required result is a function of $\ln(t)$.

Thus we apply the following algorithm to filter the digitized signal. The analog signals are sampled at equal time intervals. A simple moving average is applied to the digitized data. However, the number of points in the moving average is increased roughly as square root of the number of sampled points. This easily implemented routine does not significantly affect the final result.

III. STEADY-STATE CAPACITANCE

Before detailed measurement of the transient behavior of a device is made, it is important to make steady-state capacitance measurements as a function of voltage, frequency, and temperature. This identifies samples suitable for transient capacitance measurements. A necessary condition for the use of a capacitance measurement to determine properties of gap states is that their population change in a time short compared with the inverse of the measuring frequency. This is so that the depletion width, determined by the gap state occupancy, can follow the modulation voltage. Because thermal emission of a carrier from a gap state to a conducting state is the limiting process, this requirement places a lower limit on the measurement temperature. Unless otherwise noted the measuring frequency is 10 kHz. From capacitance measurements it is possible to determine the position of the Fermi level at the edge of the depletion region, the space-charge density, the density of states at the Fermi level, and the uniformity of the space-charge distribution.

A. Schottky-barrier and *p-n* junction devices

For doped devices, capacitance-voltage (C-V) measurements usually have a straightforward interpretation. However, for undoped devices, C-V as well as DLTS measurements, present special problems. There has been considerable discussion[24] of capacitance measurements on a-Si:H Schottky-barrier devices. It is this structure that has been widely used for gap state spectroscopy of doped a-Si:H.

An example of the temperature dependence of the capacitance is shown in Fig. 4, where the reverse bias capacitance of a Schottky-barrier device is plotted as a function of temperature. The undoped a-Si:H used for this device was grown in a high-purity system of the type used to make solar cells. Even though no dopant was added, residual states place the Fermi level slightly above midgap. Therefore, the depletion width is determined by states lying near midgap. Because these states cannot follow the measuring frequency near room temperature the measured capacitance is equal to the geometrical capacitance. Only at temperatures considerably above room temperature is the capacitance determined by gap states. In this regime the capacitance increases indicating a decrease in the depletion width. It is difficult if not impossible to analyze the capacitance-voltage curves to extract gap state densities for this sample in the usual way.

Nevertheless, a recent approach[22] using the temperature dependence of the capacitance can be used to determine both the position of the Fermi level, E_F, and the density

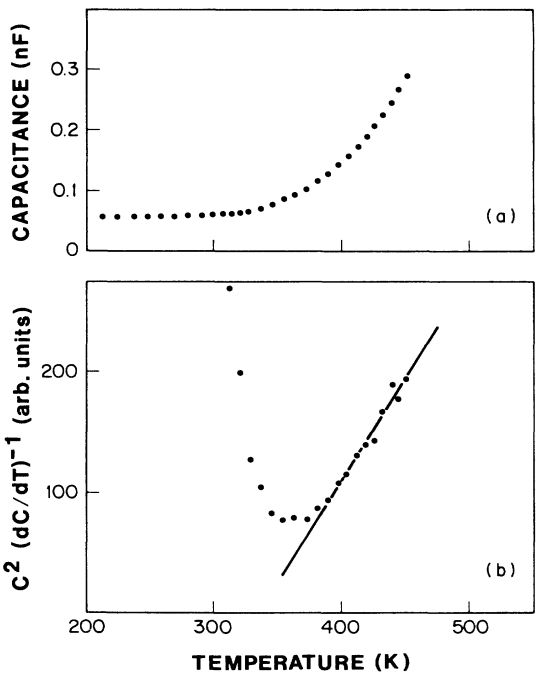

FIG. 4. Determination of $N(E_f)$ from the temperature dependence of the capacitance. (a) Capacitance vs temperature on a 2.6-μm undoped i layer at 3 V reverse bias and 10 KHz. (b) The data for (a) replotted in a form to determine $N(E_F)$. The slope of the straight line through the data gives $N(E_F)$.

of states, $N(E_F)$, at the Fermi level. We have used this method to find $N(E_F)$ in a number of samples and have found a good correlation between this density and the space-charge density determined by other means.[25] In Fig. 4(a) the curve shows the temperature dependence of the capacitance of a Schottky-barrier solar cell with an undoped layer 2.6-μm thick. The capacitance increase at higher temperatures is due to increasingly deeper states being able to respond to the measuring frequency of 10 kHz. As pointed out in Ref. 22, a plot of the function $C^2/(dC/dT)$ versus T can be used to determine $N(E_F)$. In Fig. 4(b) the curve is a plot of this function. Its slope gives an $N(E_F)$ of $(6\pm2)\times10^{+14}$ cm^{-3} eV^{-1} for this sample. This was actually one of the lower density of states that we measured. Most undoped material has $N(E_F)$ in the range of $(1-5)\times10^{+15}$ cm^{-3} eV^{-1}.

The position of the Fermi level is determined from the frequency dependence of the temperature, T_m, of the minimum of the function in the curve of Fig. 4(b). This minimum shifts to lower temperature with decreasing frequency because deeper states are able to follow the measuring frequency. The slope of a plot of the logarithm of the measurement frequency versus $1/T_m$ gives the Fermi level. For this sample, $E_F=0.71$ eV which is a common value for low-impurity density material. Fermi levels farther removed from the conduction band are most probably due to compensating impurities such as boron. In fact we have found that adding increasing amounts of boron to the i layer shifts the Fermi level continuously from 0.7 to 1.1 eV while the sample remains n type. This is because the boron compensates the a-Si:H and moves E_F toward the valence band. Accompanying this is an increase in $N(E_F)$.

B. *p-i-n* junction devices

The interpretation of C-V measurements in high-quality p-i-n or n-i-p solar-cell structures is more complex than for a Schottky-barrier structure. This is because there is not usually a well-defined depletion width in the i layer. To illustrate this we compare capacitance measurements on a p-i-n solar cell with a high-purity i layer to those on one with a doped i layer. In thin, 1 μm or less, high-purity i layers, the space charge is insufficient to cause the electric field to change significantly across the i layer.[26] The depletion widths are actually in the n and p layer. The potential energy diagram of this idealized p-i-n structure is shown in Fig. 5. In fact it is these doped layers that supply the space charge to support the uniform field in the i layer. Therefore, a capacitance measurement mainly senses changes in the depletion widths in the doped layers. Nevertheless, because these depletion widths are determined self-consistently by the charge in the i layer as well as that in the doped layers, capacitance measurements can be used to determine an upper limit to the density of space charge in the i layer.

The depletion width, W, that is determined by a measurement of the capacitance is given by the sum of the thickness of the i layer, L, and the depletion widths, W_{sn}, and W_{sp}, in the n and p layers, respectively. Finding[26] these depletion widths as well as the uniform part of the field is a straightforward application of Poisson's equation. For illustrative purposes, we assume an idealized model with the space-charge densities uniformly distributed throughout the various layers and abrupt junctions. If ρ_n, ρ_s, and ρ_p are the densities of space charge in the n, i, and p layers, respectively, then the total depletion width, $W=L+W_{sn}+W_{sp}$, is

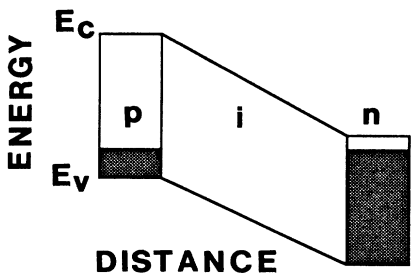

FIG. 5. Idealized potential energy diagram for a p-i-n solar cell.

$$W=L(1+\alpha VL^{-2}+\rho_s/\beta)\ , \tag{5}$$

where

$$\alpha=(1/\rho_p+1/\rho_n)Q/\epsilon \tag{6}$$

and

$$\beta=(1/\rho_p-1/\rho_n)\ . \tag{7}$$

The voltage across the cell is V, Q is the magnitude of the electron charge, and ϵ is the dielectric constant. This expression for the depletion width applies as long as $L\gg(L-W)$, the space-charge densities in the doped layers are not equal, and the space-charge density in the i layer is much less than the space-charge density in the doped layers. All these conditions are met in practice.

The most striking property of Eq. (5) is that the depletion width varies linearly with voltage instead of as the square root of the voltage as in a Schottky barrier. A particularly good example of this behavior[26] is given in Fig. 6 where the linear dependence of W and V is seen

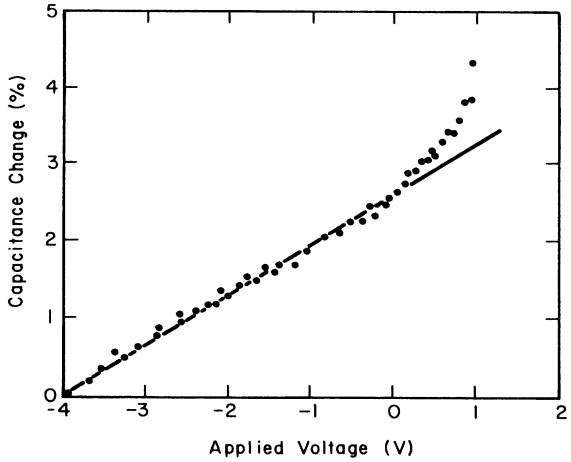

FIG. 6. Fractional capacitance change in a p-i-n solar cell vs bias. The i layer is 0.5-μm thick and the measuring temperature and frequency are 250 K and 20 Hz, respectively.

to hold over a large voltage range. It is noteworthy that the entire capacitance change over this range is only 3%. This is not seen in all cells, only the high quality ones. These measurements were made at 250 K to minimize the effects of diffusion capacitance[27] in forward bias. At higher temperatures, there is a rapid increase in the forward bias capacitance. However, the reverse bias capacitance does not increase significantly until temperatures in the neighborhood of 450–500 K where injection of electrons and holes from the doped into the i layer gives a large capacitance contribution, even in reverse bias. This is similar to the large photogenerated capacitances that are often observed in these cells.[28]

Equation (5) can be used to analyze the data in Fig. 6 to find α, which is related to the doping density. We find that

$$\rho_p\rho_n/(\rho_n+\rho_p)=3.4\times10^{+16}\ \text{cm}^{-3}\ . \tag{8}$$

We could not separately measure the space-charge densities in the doped layers. Although, the dopant concentrations were similar in the two layers, the space-charge densities can be markedly different. For the films produced by dc glow discharge at RCA, the acceptor density was usually found to be less than the donor density. Under these conditions Eq. (8) gives the space-charge density in the p layer. This is most reasonable because in a separate investigation of boron-doped a-Si:H we found that the amount of incorporated space charge can be orders of magnitude less than the amount of boron in the film.

If the space charge in the i layer is large enough, it will cause band bending in the i layer and reduce the total depletion width. The condition for this is that the total charge in the i layer be on the order of the total charge in the depletion widths in the doped layers. This condition can be written as

$$\rho_s\cong(W_n\rho_p+W_p\rho_p)/L\ . \tag{9}$$

For the example in Fig. 6, at 1 V the depletion widths are less than 1% of the i layer thickness. The highest space-charge density in the n layer is no more than about $2\times10^{+17}$ cm^{-3}. Therefore, the space charge in the i layer would have to be greater than about $2\times10^{+15}$ cm^{-3} to be just observable. In high-quality solar cells the space charge is usually less than this.

As a contrast to the above result for an undoped i layer, Fig. 7 shows the C-V characteristic of a p-i-n cell with an i layer containing 25 ppm boron. Even at this high boron concentration the i layer is still n type. The density of space charge in the i layer can no longer be neglected. It approaches the level in the doped layers. Figure 7 shows a large capacitance change in a small voltage range, typical of a depletion width forming in the i layer. The data indicate a space-charge density of $1.1\times10^{+17}$ cm^{-3}. The measurements had to be made at high temperature to insure for this measuring frequency, that the electrons could follow the capacitance signal. Detailed measurements of the frequency and temperature dependence of the capacitance, as discussed for Fig. 4, showed that the Fermi level lies about 1.1 eV below the conduction band. The Fermi level is reduced below its usual value of about 0.7 eV in undoped material by the presence of the boron.

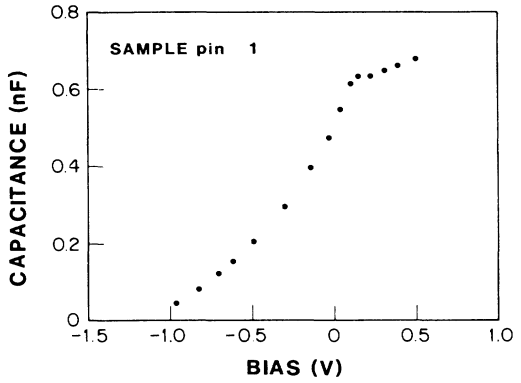

FIG. 7. Capacitance vs voltage measured at 404 K for a p-i-n solar cell measured at 1×10^6 Hz.

In solar cells, the doped layer, through which the light enters, is made as thin as possible, usually less than 100 Å. For the doping densities found in a-Si:H this thickness of doped layer can be fully depleted at moderate voltages. For example, if the space-charge density is only $1\times10^{+17}$ cm^{-3}, then the layer is depleted for voltages above 0.1 V. If one of the layers is depleted, then its effect on the capacitance is negligible since there is no band bending in it. This is fortunate, since one now knows which layer contains the depletion width. This can have important consequences for DLTS measurements as we shall discuss in the next section. Even if one of the doped layers is depleted, the depletion width can still vary linearly with voltage. However, the slope of the depletion width versus voltage curve will be different. Equation (5) can still be used by taking the limit that the space-charge density for the depleted layer tends to infinity. In this situation Eq. (5) permits an unambiguous determination of the space-charge density in the undepleted doped layer.

The above discussion shows that under certain conditions, capacitance measurements can be used to obtain parameters of the defects. If the doping is sufficiently high in a Schottky barrier or p-n junction device, then the usual depletion width analysis will suffice and the spatial density profile can be determined. In p-i-n or n-i-p devices the situation is complex. Assumptions have to be made and special conditions met to analyze the measurements and determine properties of the i layer. One assumes that the space-charge densities are uniformly distributed in the various regions. Even with this condition met it is not possible to determine the spatial distribution of the space charge.

IV. TRANSIENT EFFECTS

In this section we present results of changes in the capacitance, photocurrent, J_p, derivative of the photocurrent with respect to voltage, dJ_p/dV, and open-circuit voltage, V_{OC}. All of these can be used to characterize the defects. Although the latter three directly measure solar-cell properties, only the capacitance can be used to determine the sign and density of the trapped charge. For this reason,

most of the results are from capacitance measurements. Since the transients can be used to determine the signature, the activation energy, of the defect, it is a powerful diagnostic tool to combine measurements of the different transient effects on the same device.

A. Capacitance changes

In capacitance transient DLTS measurements, one perturbs the system by changing the space charge in the depletion width of the device. This is usually done by charge injection, using a forward bias voltage pulse. Schottky-barrier devices, however, behave differently from *p-i-n* and *n-i-p* solar-cell devices under the action of a forward bias pulse. The Schottky-barrier device permits only majority carrier injection, placing a severe limit on the amount of charge that can be injected. The maximum injected charge is limited by space-charge considerations to be less than the product of the depletion width capacitance and the voltage. Because both signs of carriers can be injected in a *p-i-n* or *n-i-p* device no such restriction applies. For this reason it is much easier to degrade a *p-i-n* solar cell with forward bias[14,15] than a Schottky-barrier cell. This is not always appreciated and is presumably the reason for the failure to observe the same amount of solar-cell degradation owing to current flow in a Schottky-barrier cell[29] as in *p-i-n* solar cells. Using transient degradation techniques described in this paper it is possible to observe small amounts of degradation. Under ideal conditions a change of as little as 0.1% in the solar-cell properties can be detected.

The usual DLTS analysis of capacitance transients, which applies to Schottky-barrier devices, is not usually appropriate for the *p-i-n* structure. To demonstrate this we first consider an ideal model in which the *i* layer is relatively defect free and that degradation produces a uniform but small amount of space charge throughout all the layers. After explaining the consequences of these assumptions, we describe the changes when these conditions are relaxed.

If the space charge in the *i* layer is small then it will produce a weak band bending. Nevertheless, the change in the band bending in the *p* and *n* layers, required to balance the charge change in the *i* layer is sensed in a capacitance measurement. To calculate the change in capacitance or depletion width produced by a charge change in the *i* layer we use Eq. (5) to find the depletion width. Let the change in charge density in the *i* layer be $\Delta\rho_s$, in the *p* layer $\Delta\rho_p$, and in the *n* layer $\Delta\rho_n$. The assumption of uniform degradation requires that

$$\Delta\rho_s = \Delta\rho_n = -\Delta\rho_p \ . \tag{10}$$

Here we assumed that the *i* layer is *n* type. Since the *i* layer is much thicker than either of the depletion widths, it will contain the bulk of the charge produced by the stress. Equation (5) can be used to find the change in the depletion width, ΔW, produced by this change in space charge. The fractional capacitance change, $\Delta C/C$, is related to the fractional change in the depletion width by the relation

$$\Delta C/C = -\Delta W/W \ . \tag{11}$$

The overall change in the depletion width is due to processes that can be considered separately. First there is the change in charge in all three layers due to charge trapping. Then there is change in W_p and W_n required to nearly balance the charge change in the *i* layer. Finally W_p and W_n readjust self-consistently with Poisson's equation. This latter effect gives the smallest change in W. The change in capacitance can be estimated using Eq. (5). To first order it is

$$\Delta C/C = -\Delta\rho_s\beta[1+\mathrm{O}(W_p/L)]/2 \ . \tag{12}$$

The significant result of this expression is that the sign of the capacitance change, relative to the sign of the charge change depends on the relative concentrations of space charge in the doped layer (through the quantity β). The physical reason for this is that the charge change in the *i* layer must be balanced by movements of the depletion widths in the doped layers. Consequently the layer with the lower space-charge density will have the larger depletion width change and will thus determine the capacitance change. For the special case of equal space-charge densities in the *n* and *p* layers higher-order terms must be included in Eq. (12). Since this special situation is not met in practice we shall not consider it further.

For example, if electrons are trapped in the *i* layer, $\Delta\rho_s$ and $\Delta\rho_n$ are negative and $\Delta\rho_p$ is positive. Thus W_n will increase and W_p will decrease. If $\rho_n < \rho_p$ then W_p decreases less than W_n increases so that the capacitance decreases. We would have the same result if the *p* layer were fully depleted. This result is the same as that for an *n*-type Schottky barrier. If electrons are trapped in a Schottky barrier then the capacitance decreases because there is now less positive space charge contained in the depletion width. On the other hand, if $\rho_n > \rho_p$ or the *n* layer is depleted, then the depletion width in the *p* layer must accommodate the charge change in the *i* layer and W_p decreases and the capacitance increases in contrast to the Schottky-barrier case.

In typical *p-i-n* solar cells the light enters the *p* layer which is made thin so it is depleted. These should act like *n*-type Schottky-barrier cells. The *n-i-p* cell on the other hand has a thin *n* layer where the light enters. It should give the opposite capacitance change. To iterate then, for solar cells, electron trapping in a *p-i-n* cell should result in a *decrease* in the capacitance. Electron trapping in an *n-i-p* cell should give an *increase* in the capacitance. Of course hole trapping gives just the opposite result from electron trapping. Thus the sign of the capacitance change can tell the sign of the trapped charge. Although transient capacitance measurements permit the sign of the charge to be measured, all spatial resolution is lost.

If the condition of uniform charge trapping is relaxed, then the above results change somewhat. There is evidence[30] that doping increases the production of light-induced defects. If we assume that all the charge change arises in the doped layers then, as above, the movement of their depletion widths determines the capacitance changes. Since the *n* layer in the *n-i-p* device is depleted it acts as a *p*-type Schottky-barrier cell. In this case electron trapping produces an increase in capacitance and hole trap-

ping a decrease in capacitance. The p layer is depleted in the p-i-n cell so that it acts like an n-type Schottky-barrier cell. Thus, in both cases, the sign changes will be the same as for the above assumptions of uniform trapping.

In support of the above ideas we present experimental results on p-i-n and n-i-p solar cells containing similar i layers. If the same types of defects are produced in the two cells, then their capacitance changes following degradation should be of opposite sign because only the depletion width in the n layer moves in the p-i-n cell and only the depletion width in p layer moves in the n-i-p cell.

Figure 8 shows a capacitance transient following degradation by a 2-V forward bias voltage pulse in an n-i-p solar-cell structure. Since the n layer is thin and presumably depleted, the depletion width in the p layer controls the capacitance change. The data show an increase in the capacitance following degradation. Therefore, the depletion width, W_p, decreased resulting in a decrease in the net negative charge in the depletion width of the p layer. Thus there was an increase in the negative charge in the i layer demonstrating that electrons were trapped. If electrons were trapped mainly in the p layer there would also be a decrease in W_p and thus an increase in capacitance.

Under similar conditions it is reasonable to expect electron trapping in a p-i-n device. In contrast to the above, however, the capacitance would be expected to decrease, irrespective of whether the dominant trapping is the i layer of the n layer. This is because the p layer is depleted in these devices. Figure 9 is an example of this.

These results were independently confirmed in Schottky-barrier and n-p junction devices[15] where the sign of the trapped charge can be unambiguously determined. An example of this is given in Fig. 10 for p-i-n cell pin 1 which has a doped i layer. This device, as discussed previously, behaves like an n-type Schottky-barrier cell. Thus we can unambiguously determine the sign of the trapped charge. Here the capacitance decreases upon degradation showing that electrons are trapped. We shall further support these interpretations of the sign of the charge that produces the capacitance changes in p-i-n and n-i-p devices when we discuss the DLTS measurements. Additional arguments will be given that the same states are responsible for trapping charge in the different devices.

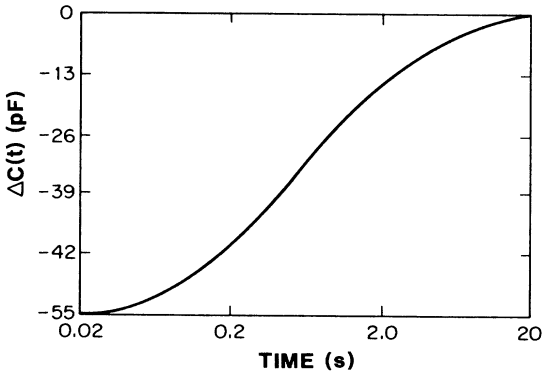

FIG. 9. Chance in capacitance following a 0.1-s forward bias voltage pulse applied to a p-i-n solar cell at 441 K.

Hole trapping can also be observed in a-Si:H. To observe the trapped holes, measurements must be made at high temperature using long degradation pulses. Hole trapping in p-i-n structures results in a capacitance *increase* and a capacitance *decrease* in n-i-p structures.

An example of hole trapping observed with long degradation times is given in Fig. 10 for sample pin 1 with the n-type i layer. The capacitance transient can be separated into two distinct portions. The initial part of the transient following degradation shows a *decrease* in the capacitance. The capacitance returns rapidly to its initial value, increases further, and finally decays to its initial value. The initial change is due to a large number of electrons being trapped. At longer times these have been thermally emitted leaving the more tightly bound holes in the device. Finally, at very long times the holes are thermally relaxed. Because the time constants for these two decay modes are over an order of magnitude different they can be easily separated.

The time constants for the two decay modes in Fig. 10 are plotted versus the inverse of the temperature in Fig. 11(b). From the slope and intercept on this Arrhenius

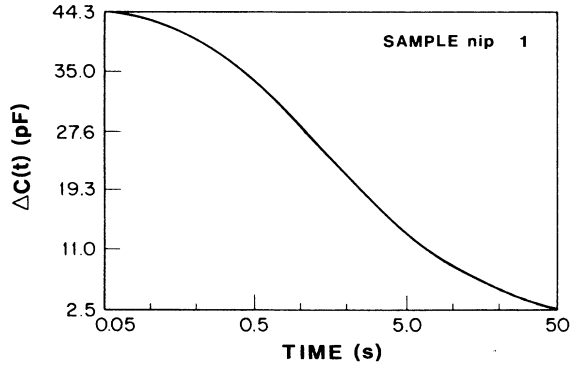

FIG. 8. Change in capacitance following a forward bias voltage pulse applied to an n-i-p solar cell at 470 K. Measured at a reverse bias of -0.1 V.

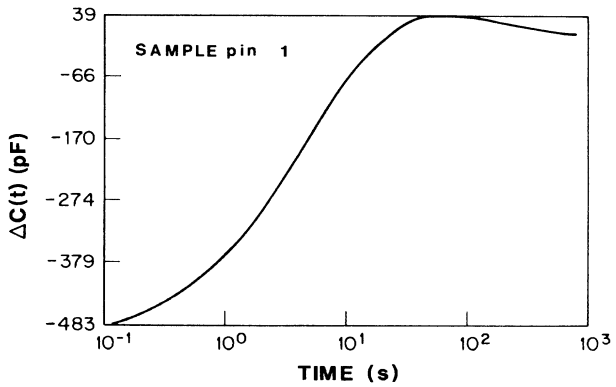

FIG. 10. Chance in capacitance following a 400-s forward bias voltage pulse for a p-i-n solar cell with a doped i layer at 434 K.

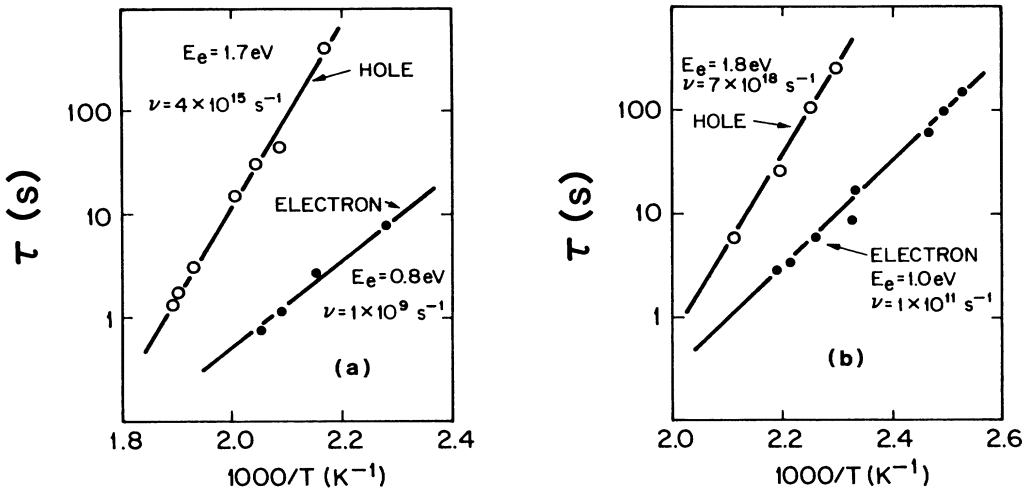

FIG. 11. Logarithm of the emission time plotted vs inverse temperature. (a) Cell nip 1. (b) Cell pin 1. "Electron" and "hole" refer to the sign of the trapped charge.

plot, the emission energy and attempt-to-escape frequency can be determined. The process leading to a capacitance decrease has a low activation energy of 1.0 eV and a ν of $1\times10^{+11}$ s^{-1}, whereas, for the capacitance increase $E_e=1.8$ eV and $\nu=7\times10^{+18}$ s^{-1}. Since this is a Schottky-barrier-like structure, the capacitance *increase* must be due to hole capture and the capacitance *decrease* to electron capture. Thus hole and electron trapping can be identified by their emission energies. This identification is very useful when it is not possible to measure the sign of the charge such as in V_{OC} and J_p transients. In Sec. VII we use this identification to explain some puzzling results in the literature.

The results for the *n-i-p* structure are entirely consistent with the above. A degradation produced capacitance decrease with its high-emission energy is to be associated with hole capture. The capacitance increase is to be associated with electron capture and a lower-emission energy. The same measurements as described above were carried out on *n-i-p* sample nip 1 to determine the activation energies for electron and hole emission. The results are displayed in Fig. 11(a). They show the same pattern for emission energies as for sample pin 1. Namely that the hole has a higher-emission energy than the electron.

Later we will give a reasonable explanation for the magnitudes of these energies and attempt-to-escape frequencies. Now we want to point out only that the signs of the capacitance change and the parameters of the decay times are entirely consistent with the picture of the response of the *p-i-n* or *n-i-p* solar cell to charge trapping in the *i* layer.

We have not been entirely successful in observing significant hole trapping in *n*-type metal Schottky-barrier devices for two reasons. One is that the majority of the degradation was carried out using current pulse. This precludes hole injection. The second is that even with light degradation, we did not degrade long enough or carry out the measurements at high enough temperature. As Fig. 10 shows, long degradation times are necessary to observe the hole signal.

Before leaving this section we wish to point out another difficulty with interpretation of measurements on *n-i-p* or *p-i-n* devices. If both doped layers are thin enough, it is possible to fully deplete both layers leading to further ambiguity of interpretation. Figure 12 shows the bias dependence of the capacitance change caused by forward bias degradation of an *n-i-p* cell. In far reverse bias it is possible to deplete both layers so that the device acts like an *n*-type barrier cell (the *i* layer is *n* type). In this case a trapped electron would produce a decrease in capacitance. This is just what is observed. Nevertheless, at small reverse bias a depletion width forms in the *p* layer so that the capacitance increases for electron trapping. DLTS analysis of this cell shows that $E_e=0.87$ eV which is characteristic for the electron trap. Even if the bias is 0 the potential drop in the *i* layer is still negative because of the builtin potential of about 0.6 V in these devices.

B. Current and voltage changes

The photocurrent and open-circuit voltage usually decrease under light or current degradation. However, there is only an indirect connection between their changes and the change in the density of defects. The connection depends on the model (of which there are many) of the photovoltaic process. Nevertheless, these quantities do sense the presence of the defect so that their transient changes can be used to find E_e. If J_p is a weak function of the defect density, then dJ_p/dV will be a more sensitive probe. Furthermore, dJ_p/dV is a direct[31] measure of the density of recombination centers which presumably increase under degradation. Also, using strongly absorbed light to measure the photocurrent, regions near the interfaces can be probed. This can give information in addition to that obtained using uniformly absorbed light which averages over defects produced throughout the device.

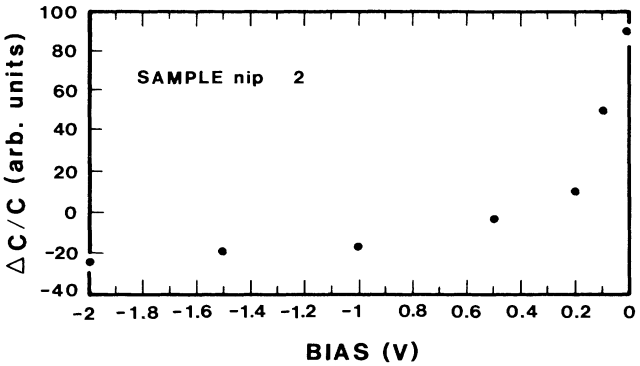

FIG. 12. Bias dependence of the initial capacitance change for an *n-i-p* cell. The cell was degraded with 690-nm light at 440 K.

V. DEGRADATION

Before presenting the DLTS results we discuss device degradation in some detail. A striking feature of degradation is that the production rate for the defects is thermally activated.[15] At least for any devices that I have studied this has been the case. This appears to be the chief reason for the exceedingly low MSD production rate at room temperature.

We have found that either light, absorbed in the cell, or foward bias current pulses produce defects with the same characteristics; i.e., charge, E_e, and ν. Nevertheless, under some conditions the same kind of degradation can produce trapped electrons and holes. For example, forward bias current degrades *p-i-n* solar cells producing an excess of trapped electrons if the degradation time is short. However, prolonged degradation at high temperature produces an excess of trapped holes. The same applies for a uniformly absorbed light.

There is little if any evidence for saturation or complete production of all possible defects at room temperature. The most common observation is that, under steady irradiation, the density of defects or the amount of degradation increases logarithmically with time with no saturation. This failure to fill all the defects may be due to the exceedingly slow rate of degradation at room temperature. Nevertheless at high temperature, the degradation rate is so fast that all the defects can be filled in a short time. In fact first-order kinetics are often obeyed. The amount of degradation increases linearly with time until saturation.

An example of this is shown in Fig. 13(a) where the amount of degradation of an *n-i-p* solar cell is plotted versus time of illumination. The amount of degradation was determined by measuring the fractional capacitance change and making the assumption that degradation is proportional to the density trapped electrons. Since the capacitance change is positive, the defects trap electrons. The data show a linear increase in defect density with time followed by a saturation. The saturation in this case is not caused by filling all the defects, but rather by reaching a steady-state condition where the number of defects produced per unit time is equal to the number of defects removed per unit time. At the highest temperature ΔC decreases slightly because of the onset of hole trapping.

It is obvious from Fig. 13(a) that the rate of defect production increases dramatically with increasing temperature. This behavior is always observed for these defects at elevated temperature whether they are produced by light or current. The slope of the linear portion of the curves is the production rate p_d. In Fig. 13(b) the logarithm of P_d is plotted versus the reciprocal of the absolute temperature. The Arrhenius behavior of P_d shows that it is thermally activated with an energy, E_p, of 1.23 eV. Not only can one determine the activation energy from the slope of the degradation versus time curve, but it can be determined from the temperature dependence of the sa-

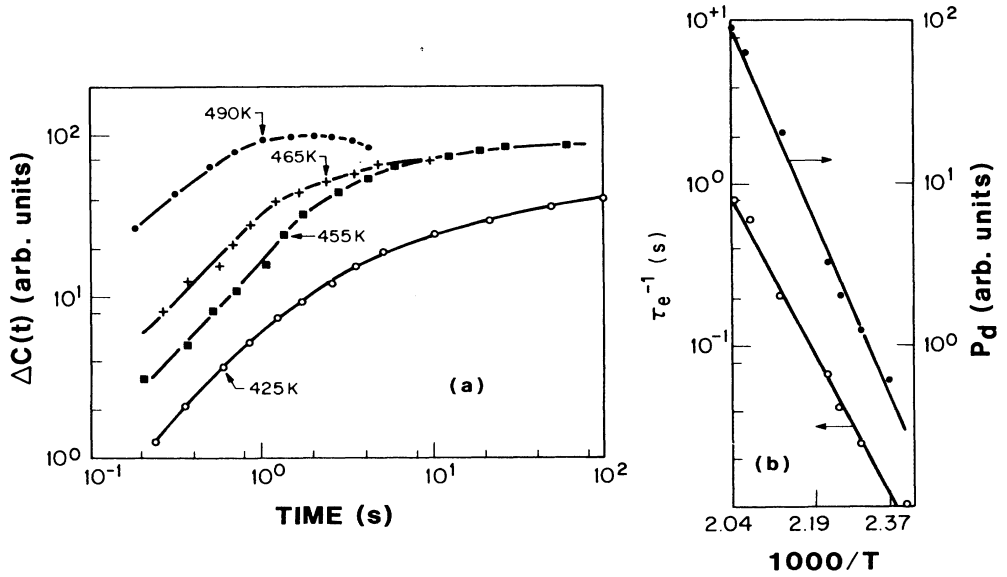

FIG. 13. (a) Change in capacitance of cell nip 3 due to 690-nm radiation from a krypton laser plotted as a function of the logarithm of the time of for a variety of temperatures. (b) Arrhenius plots of the production rate P_d, and $1/\tau_e$ vs 1000/T.

turated portion of the curves in Fig. 13(a) as we now show.

A peculiar property of the MSD is that the number produced in the steady state increases with increasing temperature. For a normal system, one expects that the number of defects produced in steady state would *decrease* dramatically at high temperature where they anneal much faster. The data in Fig. 13(a), however, show just the opposite effect. The number of defects in the steady state increases with increasing temperature.

The time dependence of the production of the defects can be found from a simple first-order model which is

$$\frac{dN_s}{dt} = P_d - N_s/\tau_e \ , \tag{13}$$

where N_s is the number of defects, and τ_e the emission or decay time for the defect. The solution of this equation is

$$N_s = \tau_e P_d [1 - \exp(-t/\tau_e)] \ . \tag{14}$$

At short time N_s increases linearly with slope tP_d. For the steady state, $t/\tau_e \gg 1$, $N_s = \tau_e P_d$. The characteristic time to reach the steady state is τ_e. Since this is the annealing time for the defect, it should decrease with increasing temperature. This is clearly shown in Fig. 13(b) where it is seen to be thermally activated. The activation energy $E_e = 1.09$ eV.

If P_d were weakly temperature dependent, as is normal for electron or hole capture in semiconductors, then the linear slopes, P_d, of the curves in Fig. 13(a) would all be nearly the same. Note that the slope is given by the magnitude of the ln-ln plot. However, there is a dramatic increase in slope with increasing temperature showing the strong thermal activation of P_d.

The small difference in the activation energies for production and annealing appears to be a universal property of these defects. Whenever we have been able to measure both quantities, we have found that the activation energy for production is greater, by about 10%, than the activation energy for emission.

The rate of degradation does not always follow first-order kinetics as demonstrated above. The common behavior at room temperature is a degradation that increases sublinearly with time. An example[16] of this is shown in Fig. 14. Here the capacitance as well as the short-circuit photocurrent are shown slowly changing with time of forward bias degradation. The capacitance decrease at longer time is caused by hole trapping. The change in the photocurrent shows that the degradation changes logarithmically with time. The large displacement of the photocurrent along the time axis again points out the dramatic increase in degradation rate with temperature.

A further example of the time dependence of degradation is shown in Fig. 15 for a *p-i-n* solar cell that shows rapid degradation even at room temperature. The change in the number of recombination centers produced by forward bias current is plotted versus the logarithm of the degradation time. The change in the number of recombination centers is proportional to the reciprocal of the drift length of the photocarriers.[31] The drift length is inversely proportional to the derivative of the short-circuit

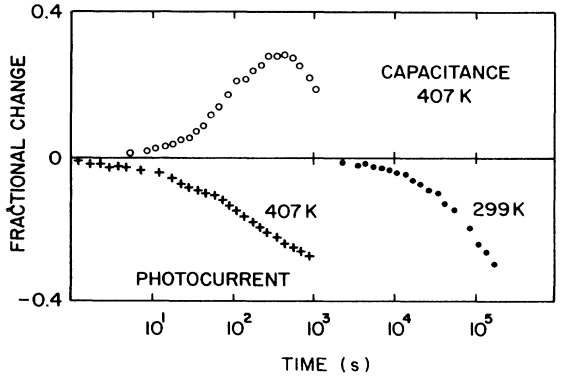

FIG. 14. Time dependence of the fractional changes in the capacitance, ○, and short-circuit photocurrent, +,●, caused by forward bias current degradation of an *n-i-p* solar cell. The photocurrent was measured at zero bias using 600-nm light. The capacitance was measured at −0.2-V bias.

photocurrent, J_{PC}, with respect to voltage. The slope dJ_{PC}/dV is proportional to the in-phase component of the ac admittance under illumination. For this example a forward bias current pulse degraded the cell. However, the same result was obtained using light to degrade the cell. It is obvious from the data that the logarithmic time dependence is obeyed over a large time interval. At short times, however, the degradation varies linearly with time.

Figure 15 also shows the dramatic increase in the de-

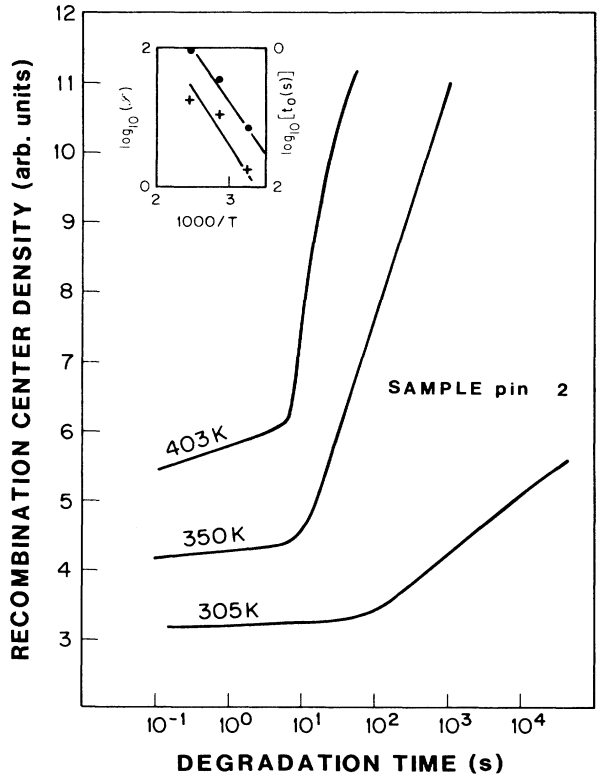

FIG. 15. Change in the density of recombination centers vs logarithm of the time of degradation at different temperatures for a *p-i-n* solar cell. Insert in the figure is a plot of the logarithm of $\mathcal{S}$ vs the reciprocal of the temperature. ●, $\mathcal{S}$, +, intercept t_0.

gradation at elevated temperature. Both the magnitude and the characteristic time t_0 for the degradation change with temperature. t_0 is the intercept of logarithmic part of the data on the time axis. Its meaning will be discussed in the next section. The insert in the figure shows the slope, $\mathcal{S}$, of the straight-line portion of the data on an Arrhenius plot. It is seen that it is thermally activated with an activation energy of about 0.3 eV. On the same plot, t_0 is shown. It is activated with about the same activation energy. Measurements of the temperature dependence of the degradation at elevated temperature on other samples show that it increases exponentially with increasing temperature.[15] This behavior appears to be a universal feature of the MSD. Most of the data for solar-cell degradation can be plotted in this manner to yield a $\ln(t)$ dependence.

The data in Fig. 15 are typical of that for an unstable solar cell. It can be rapidly degraded at room temperature using moderate current pulses. One reason that it is particularly unstable is that it contains about $1\times10^{+18}$ cm^{-3} carbon in the i layer. Carbon in a-Si:H forms a defect that can be removed by annealing at room temperature.[17]

Even though degradation in Figs. 14 and 15 does not show saturation in time near room temperature, a steady-state condition with the number of defects produced per unit time equal to the number of defects removed per unit time can be readily attained at elevated temperature as was shown in Fig. 13(a). Although, there can be a saturation in the degradation with time at a particular temperature, this does not necessarily mean that all the possible defects have been produced. The saturation usually means that the steady state has been reached. Only if the amount of steady-state degradation saturates with the strength of degradation can one be certain that all the defects have been produced. An example of this is given below.

The data in Fig. 13(a) show that steady-state conditions can be obtained at long time of degradation. The time to saturation only depends on the emission time. If first-order kinetics are obeyed, as the data indicate, then the steady-state density of defects should increase with the strength of the degradation until all the defects are formed. Data supporting this are shown in Fig. 16 where the fractional change in capacitance, measured at long times in the steady state is plotted versus the irradiation flux. Clearly the data show a saturation and demonstrate that all the possible defects have been produced.

These measurements are exceedingly difficult to make at lower temperature for two reasons. One is the long time to reach the steady state because the emission time is thermally activated. The other is that higher light fluxes must be used at lower temperature. In the steady state $N_s=\tau_e P_d$. Because P_d has a higher-activation energy than τ_e, the number of defects produced at a given light flux decreases at lower temperature.

I want to close this section by emphasizing the point that my measurements determine the change in MSD density. As we previously showed[16,20] and will discuss again in Sec. VII, the MSD's are in equilibrium at high concentrations at elevated temperature. This fact is receiving a great deal of attention at present.[32] It is possible[16,20] to remove, in reverse bias, the equilibrium population of MSD's. Thus one cannot only measure the absolute number of MSD's present in equilibrium at any temperature, but also measure the absolute number produced by the various stresses.

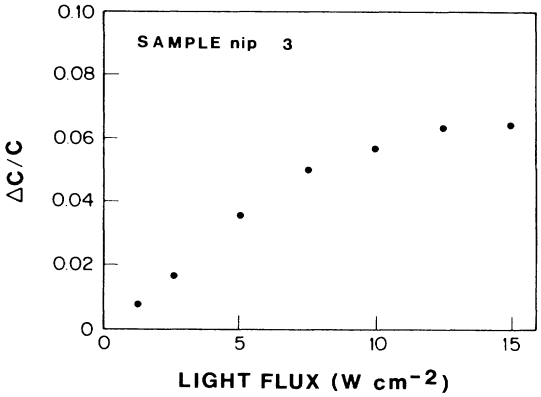

FIG. 16. Measure of number of electrons trapped to form a steady-state population of metastable defects produced by illumination of an n-i-p solar-cell device with 690-nm radiation from a krypton laser at 463 K as function of light flux using a 10-s stress pulse.

VI. ANNEALING

Although we have discussed DLTS results in previous sections we wish to amplify some of the topics and present some new data. As shown in Sec. IV, capacitance changes can give the sign and density of the trapped charge and the E_e of the MSD. Transient changes of photovoltaic properties can only determine the emission energy and, depending on the model used, the density of defects. It is possible that some of the effects observed by transient capacitance measurements are not necessarily involved in solar-cell degradation. Nevertheless, whenever we have been able to make simultaneous measurements of the changes in capacitance and photovoltaic properties, the emission energies are nearly the same.

The majority of the results that we shall present are for voltage pulse degradation. This is mainly for convenience. We have not been able to find a significant difference between the properties of defects produced by voltage pulses or by uniformly absorbed light. One such property is the activation energy for annealing of the defect. This is a signature of the defect since different defects would have different activation energies. Figure 17 shows the capacitance transient DLTS function $S(t)$, for both light and voltage pulse degradation of sample pin 1. Since $S(t)$ is positive for this n-type cell, the data show that holes are trapped following degradation. The figure shows that both current and light have the same effect.

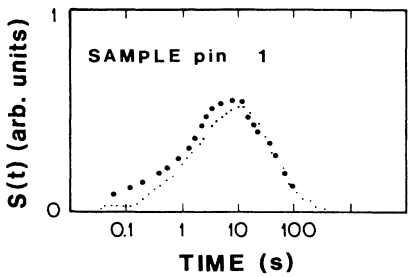

FIG. 17. $S(t)$ for both light and voltage pulse excitation of a *p-i-n* solar cell. ●●●, illumination with 690-nm light for 1 s at 474 K. · · · ·, 0.4-s forward bias pulse at 472 K. The sample was reverse biased at −5 V for both measurements. The scales are not the same.

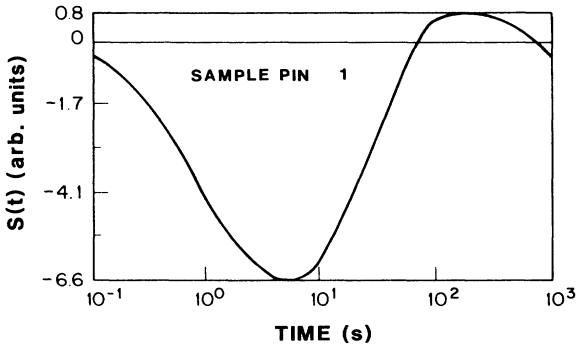

FIG. 19. $S(t)$ for capacitance transient depicted in Fig. 10.

These measurements were repeated at different temperatures to construct an Arrhenius plot yielding an emission energy $E_e = 1.8$ eV.

Usually $S(t)$ indicates a single slightly broadened energy level. Compare $S(t)$ in Fig. 18 with the calculated value shown in Fig. 2. In this case the decay transient is exponential and the emission time can be readily determined from it. Observation of a single energy level is not an isolated instance. Often a single DLTS peak is observed, even though both holes and electrons can be trapped. The reason is that for a particular temperature and degradation condition one sign of carrier is trapped more readily than the other or is emitted more easily. The *i* layer in this structure contains 25 ppm boron so that there is a well-defined depletion width in the *i* layer and the results have a straightforward interpretation. Since this is a Schottky-barrier-like structure, the capacitance *decrease* must be due to electron capture. The data in Fig. 17 for the same sample were obtained at a much higher temperature where hole emission dominates.

When more than one energy level is involved the decay transient is not exponential. Thus is it not easy to determine the emission energy from it. An example is shown in Fig. 10. The capacitance transient shows a sign change from an initial capacitance *decrease* to a capacitance *increase* after 12 s. $S(t)$ for these data is plotted in Fig. 19. Two peaks are clearly resolvable. The position of these peaks gives the emission times for electron and hole. Since the data are for sample pin 1, an increase in capacitance, positive $S(t)$, means hole trapping and a negative $S(t)$, electron trapping. The data thus show that at this temperature, most of the electrons are emitted before the holes are. As the temperature is increased, the emission times for both electrons and holes decrease. These times are shown in Fig. 11(b).

Because the emission energies for electrons and holes differ by over 0.8 eV, both emission rates are on the same experimental time scale only over a small temperature interval. Another reason that only one or the other is usually observed is that the production rates are also markedly different. If a short degradation pulse were used for the conditions of Fig. 10 only electron emission would be observed.

It is not easy to observe the hole emission signal. The rate constant for hole trapping or emission has a high activation energy. Thus high temperatures are required to observe the hole state. For a long time we concentrated on the electron state and missed seeing the hole state. The reason is because the degradation must be applied for a long time to obtain the hole emission signal. This is shown in Fig. 20 which is a series of $S(t)$ derived from capacitance transients for different times of voltage stress. The initial part of $S(t)$ is negative indicating that more electrons are trapped than holes. The electron emission time at this temperature is about 6 s so that all the elec-

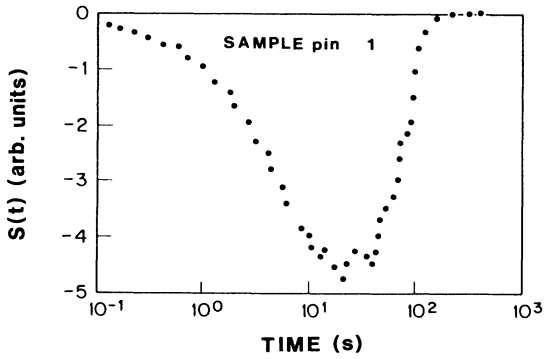

FIG. 18. Capacitance transient $S(t)$ for a *p-i-n* solar cell measured at 420 K using a 0.01-s current pulse for degradation.

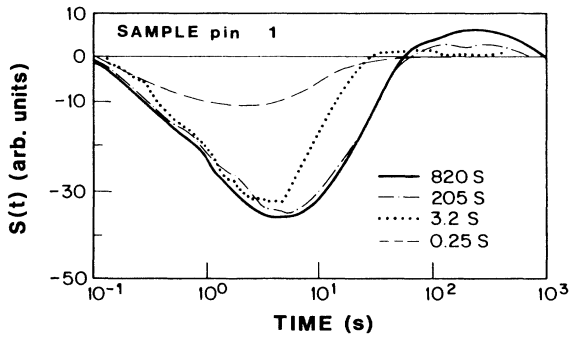

FIG. 20. Capacitance transient $S(t)$ for a *p-i-n* solar cell for different times of voltage stress. Measurement temperature is 434 K. Sample reverse biased at −5 V. Pulse voltage 0 V.

trons are emitted by 60 s when the hole signal appears. For degradation times shorter than 0.4 s the capacitance change remains negative throughout. For a degradation pulse time of 3.2 s, however, the capacitance becomes slightly positive at 80 s indicating some holes are trapped. The electron signal saturates with increasing length of degradation pulse because the steady state is reached for electron emission and production. The hole signal continues to increase out to the longest degradation time. The hole signal increases logarithmically rather than linearly with degradation time.

With increasing temperature, the peaks in $S(t)$ move closer together because the hole emission time has a stronger temperature dependence than the electron. It would normally be difficult to separate the two states. However, the rate of hole trapping increases rapidly with increasing temperature, whereas electron trapping has reached steady-state conditions. Therefore the hole signal grows and is easy to resolve from the electron signal.

For most samples $S(t)$ indicates a single slightly broadened level. However, in some samples a distribution of states can be observed. Figure 20 showed some evidence of this. For longer degradation times $S(t)$ for the electron trap increased at longer times. This can be seen by comparing the 3.2 s with the 205-s degradation time data. They show that longer degradation produces more states with a higher emission energy [$S(t)$ is proportional to the density of defect states at an energy E and E is proportional to $\ln(t)$]. Nevertheless, $S(t)$ saturates for these states at longer times as the 820-s data show. Note that the hole signal does not saturate.

Similar data are shown in Fig. 21 for the hole trap in a p-i-n sample. Here both the peak position and magnitude of $S(t)$ change continually with degradation time. The data show that for longer times, defects with larger emission energies are produced and that those with lower E_e have reached the steady state. For these data the density of defects increases as the logarithm of the degradation time. We could not find a saturation of the signal out to 1×10^4 s. This appears to be typical of the hole. For the electron we found first-order kinetics to be obeyed.

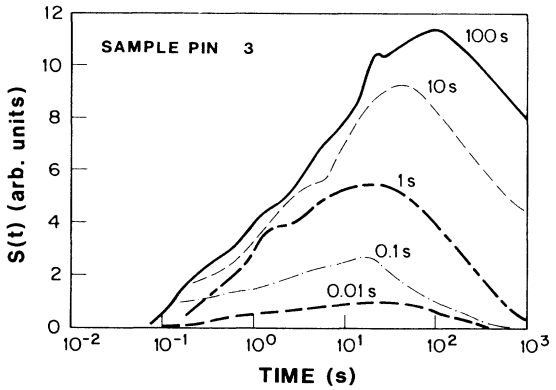

FIG. 21. Capacitance transient $S(t)$ for different degradation times of a p-i-n solar cell measured at 493 K. Sample reverse biased at -0.5 V. Pulse voltage 1 V.

Another example of a distribution of MSD can be seen in Fig. 22. Here $S(t)$ determined from the transient recovery of the open-circuit voltage is shown. For this cell, V_{OC} changes were a more sensitive probe of the MSD than capacitance changes. At short time the low-energy defects are populated until a steady state is attained. Further defect creation only serves to produce defects with a higher emission energy that have lower production and decay rates. This is consistent with the fact that all these defects have a thermally activated production rate with the activation energy for production closely related to the emission energy.

Since we have presented a number of diverse properties of MSD's determined by transient techniques it is appropriate to assemble the results in one place and see if a coherent picture results. Table I lists the sample number, the emission energy, the attempt-to-escape frequency, and the sign of the charge trapped by the MSD. The mode of degradation can be current, red (uniformly absorbed), or blue (strongly absorbed) light. For n-i-p cells the light enters through the p layer and for n-i-p cells through the n layer. Under the DLTS heading, cap means capacitance transient and V_{OC} open-circuit voltage transient. PC(r) and PC(b) refer, respectively, to photoconductivity using red or blue light. Using strongly absorbed (blue) light for photoconductivity is a means to achieve some degree of spatial localization since the photoconductivity is determined to a large extent, by recombination centers near the contact through which the light enters.[28,16] Similarly using blue light for degradation allows injection into the bulk by field-driven transport of predominantly one sign of carrier. Under the comments the doping of the i layer is indicated if applicable. These data include samples not shown in the figures.

The data in Table I for the large variety of devices fall into three distinct categories that can be grouped by E_e and ν. The first group with E_e around 1 eV and $\nu < 1\times10^{+13}$ s^{-1} is always associated with an electron trap. Another cluster of E_e's below 0.6 eV and $\nu < 1\times10^{+5}$ s^{-1} is also associated with an electron trap. These have been found only in few devices that contain large amounts of carbon or fluorine in the i or p layer. The group with $E_e > 1.4$ eV and $\nu < 1\times10^{+13}$ s^{-1} can be associated with a hole trap. The "?" mark before a charge in the table means it was inferred from the value of E_e.

The data in the table are reproduced in Fig. 23, where

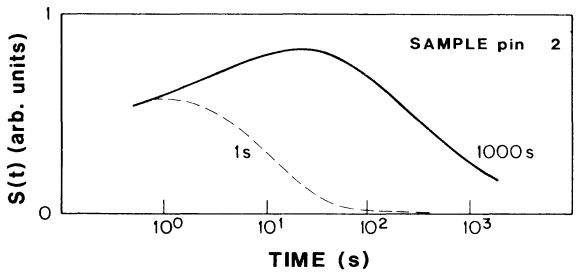

FIG. 22. $S(t)$ determined from V_{OC} on a p-i-n solar cell using voltage pulse degradation and red light to produce the photovoltage. Measured at 359 K.

the separation into three groups is clear. The data are also seen to lie along a straight line of the form $\nu = C\exp(+E_e/E_c)$ where $E_c \approx 0.043$ eV. Therefore, E_e and ν can be used as signatures for the MSD to tell what the trap is from other experiments where only E_e and ν can be measured.

In many cases both hole and electron trap MSD's can be produced in a single device, but only if both signs of carrier are present in the active layer. Examples of only one carrier producing one sign of defect are the following: for holes, when sample nip 4 was degraded using blue light, only hole trapping was observed. In this case the light is strongly absorbed in the n layer and the field is such that only holes are transported into the i layer. For electrons, current degradation of n-type Schottky barriers and p-n junctions inject only electrons.

The same kind of MSD can be produced using either current or light to degrade the device. Examples of this

TABLE I. Number of diverse properties of MSD's determined by transient techniques.

Sample number	Degradation mode	Emission energy (eV)	Attempt-to-escape frequency ($s-1$)	Charge sign	DLTS method	Comments
			n-i-p cells			
nip 1	current	0.8	$1\times10+9$	e^-	cap	
nip 1	current	1.7	$4\times10+15$	h^+	cap	
nip 2	red	0.87	$1\times10+8$	e^-	cap	
nip 3	red	1.09	$1.4\times10+9$	e^-	cap	
nip 4	red	1.67	$2.8\times10+15$	h^+	cap	F in p layer
nip 4	blue	1.63	$2.2\times10+15$	h^+	cap	
nip 4	red	0.56	$4.3\times10+3$	e^-	cap	
nip 4	current	0.51	$2.1\times10+3$	e^-	cap	
nip 5	red	1.14	$2.2\times10+9$	e^-	cap	
nip 5	current	0.86	$1.6\times10+7$	e^-	cap	
nip 6	red	1.6	$1.4\times10+15$	h^+	cap	
nip 6	red	0.81	$3\times10+8$	e^-	cap	
nip 7	current	0.85	$3\times10+7$	e^-	cap	
nip 7	current	1.78	$1\times10+17$	h^+	cap	
nip 8	red	0.8	$2\times10+8$	e^-	cap	
nip 8	red	1.4	$1\times10+15$	h^+	cap	
nip 9	current	1.01	$8\times10+8$	e^-	cap	
nip 9	current	1.03	$9\times10+8$	$?e^+$	PC(b)	
nip 10	red	1.15	$7.5\times10+10$	e^-	cap	
nip 11	red	1.3	$4.5\times10+11$	e^-	cap	
			p-i-n cells			
pin 1	current	1.0	$1\times10+11$	e^-	cap	25 ppm B in
pin 1	current	1.8	$7\times10+18$	h^+	cap	i layer
pin 1	red	1.76	$6\times10+18$	h^+	cap	
pin 2	current	0.38	$1\times10+4$	$?e^-$	V_{OC}	2 at.% C in
pin 2	current	1.1	$1\times10+10$	e^-	cap	i layer
pin 2	current	0.4	$1\times10+4$	e^-	cap	
pin 3	current	1.45	$5\times10+13$	h^+	cap	3 ppm B in i layer
pin 4	current	1.7	$2\times10+17$	h^+	PC(r)	C in p layer
pin 4	current	0.43	11	e^-	PC(b)	
pin 5	current	1.4	$1\times10+12$	$?h^+$	PC(r)	C in p layer
pin 5	current	0.3	85	$?e^-$	PC(b)	
pin 6	red	0.93	$4.4\times10+8$	e^-	cap	
pin 7	current	1.2	$9\times10+11$	$?e^-$	V_{OC}	
			barrier cells			
Shn 1	current	0.86	$4\times10+7$	e^-	cap	n-type Schottky
Shn 2	current	1.2	$2.4\times10+11$	e^-	cap	n-type Schottky
Shn 3	red	1.01	$1\times10+9$	e^-	cap	n-type Schottky
pn 1	current	0.36	$1\times10+2$	e^-	cap	p-n junction
pn 1	current	1.2	$1.2\times10+12$	e^-	cap	10 at.% C in p layer
pn 2	current	1.09	$1.5\times10+12$	e^-	cap	

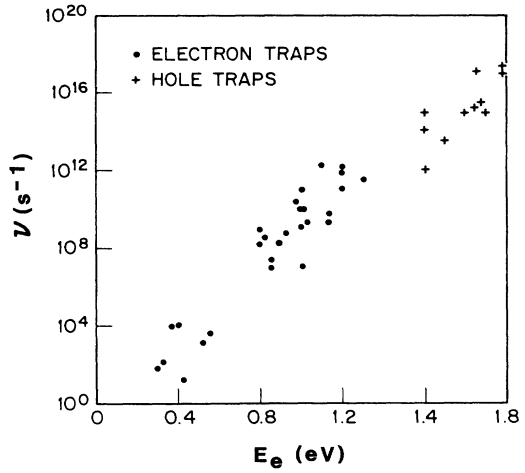

FIG. 23. Data in Table I plotted as logarithm of ν vs emission energy.

are pin 1, nip 4, and nip 5. However, when current pulses are used, holes can be trapped only if they can be injected. For this reason it has not been possible to populate hole traps in an n-type Schottky barrier[15] using current pulses. In contrast, both carriers can be trapped in a p-i-n structure because holes and electrons can be injected from the p and n layers, respectively. Examples of this are pin 1, nip 1, nip 4, nip 6, nip 7, nip 8, and perhaps pin 4. It is difficult to degrade a Schottky-barrier structure when only one sign of carrier can be injected. Charge-neutrality conditions limit the amount of space charge in the cell. If both signs of charge are injected, by voltage or light, then space charge does not limit the degradation. DLTS techniques, however, can detect small amounts of degradation because of their sensitivity.

The data in Table I also show that transient changes in photoconductivity and V_{OC} can be used in DLTS techniques to find the same MSD found by capacitance transients. This is strong evidence that both hole and electron trap MSD's cause degradation. Examples of this are pin 2 and nip 9. Another example is shown in Fig. 14 where both the change in photocurrent and capacitance are shown. Initially the capacitance increases indicating that electrons populate the MSD. However, at longer times the capacitance decreases even though the photoconductivity continues to decrease. The decrease in the capacitance shows that holes are now being trapped. Extrapolation of these data to very long time would indicate that the predominant MSD's would contain holes.

VII. DISCUSSION

A. Degradation

The data presented in the preceding sections show that device degradation or the SW effect can be produced in a-Si:H by either light or current flow and furthermore that the same type of MSD is formed by either. Both signs of charge are trapped in MSD's when uniformly absorbed light is used for degradation. If strongly absorbed light or current is used then only carriers that can be injected will be trapped. For example, only electron trap MSD's have been formed in p-n junctions or n-type Schottky-barrier devices using electron current pulses. In p-i-n devices current pulses can produce both signs of trapped charge. It is only necessary to have electrons or holes present in the a-Si:H to produce or allow the defect to trap charge. This can be demonstrated by the following experiment that shows both the similarity in activation energies for population and depopulation of the MSD as well as show that thermal electrons can produce the SW effect. It involves trapping and release of an electron in an n-type a-Si:H Schottky-barrier device. The conditions are such that electron trapping and release from the MSD is the most likely process.

The first part of the experiment[20] is shown by curve (a) in Fig. 24 which is $S(t)$ for an n-type Schottky-barrier device. It is reverse biased to produce a depletion width W_0. This negative $S(t)$ follows a short ($1s$) forward bias pulse which decreases the depletion width. This allows electrons from the bulk to flow into the region that was originally depleted and be captured by the MSD. At the end of the pulse electrons are thermally released from the MSD producing the shape of $S(t)$ in curve (a). This takes some hundreds of seconds. This is the standard type of DLTS experiment that we have discussed previously.

The second part also begins with sample reverse biased as above. However, instead of a *forward* bias pulse, a 20-s *reverse* bias pulse is applied to widen the depletion width to W_1. Defects originally occupied with electrons in the bulk low-field region are now in the high-field depletion region. Therefore, electrons thermally emitted from traps can leave the depletion region during the pulse. The pulse is applied long enough so that any electron trap MSD in the depletion with W_1 can anneal. At the end of this reverse bias pulse electrons from the bulk can flow back into the region between W_1 and W_0. If there were no barrier for their capture this would occur virtually instantaneously at this temperature. As can be seen from Fig. 24, the time constant for the trap filling is about 2 s. By repeating this type of measurement at different temperatures, the capture energy can be determined. It is 0.98 eV. This

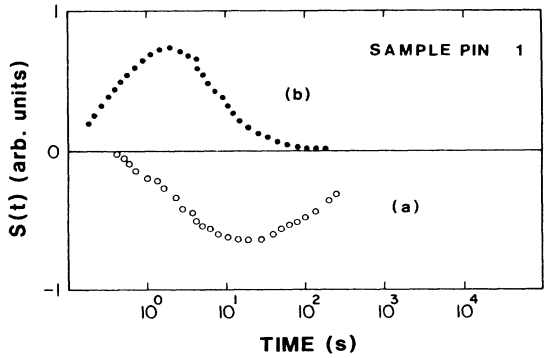

FIG. 24. DLTS functions $S(t)$ determined from transient capacitance measurements on an n-type Schottky-barrier device at 500 K using a -1-V reverse bias. The positive $S(t)$, curve (b) follows a reverse bias pulse. The negative $S(t)$, curve (a), follows a 0.5-V forward bias pulse.

high-activation energy clearly shows a barrier for electron capture.

A barrier for capture can result from two causes. One is the high barrier for production of the MSD as discussed in Sec. V. The second is an apparent barrier to capture arising from the exponential lengthening of the trap filling time owing to the low density of electrons in the space-charge region between the Schottky barrier and the edge of the depletion width. Their density decreases exponentially with the potential. If there were no other barrier to capture this alone would produce a long filling time. Analysis of this effect shows that $S(t)$ increases roughly as $[\ln(t)]^{1/2}$ until a cutoff time that increases exponentially with bias. The curve in Fig. 24 does not have this shape. Furthermore, we did not observe any change in its shape or peak position (apart from magnitude) with bias. Thus we expect that this is a small effect superimposed on the large one due to the high barrier for defect production. Since the activation energy for capture is slightly higher than the emission energy of 0.86 eV, the capture is most likely by the MSD.

Reverse biasing of the device can be viewed as the "anti SW effect" since it removes MSD's. It should be stressed that this measurement is performed on a-Si:H in the fully annealed or state A (Ref. 1) condition. This shows that there are always MSD's present in equilibrium, since they can be removed, or at least the trapped charge can be removed by the reverse bias. The presence of MSD's in equilibrium at high temperature has been recently confirmed by other means.[32]

The above experiment as well as those preceding it permit one to conclude the following about the degradation produced defects.

(1) Emission and capture are thermally activated. The emission energy is always slightly less than the capture energy.

(2) It is only necessary to have electrons present in the bulk to populate the MSD. Light is not necessary. It is thermal energy that causes the electron to populate the MSD. The same arguments can be made for the hole. The data for sample pin 1 showed that if only holes were present in the i layer then only the hole trap MSD was formed.

(3) The defects are produced in the absence of light. They are most probably present in equilibrium. In fact the MSD can be removed or depopulated by reverse bias.

Experiments similar to those described above have been carried out on a large number of a-Si:H devices, including p type and undoped, with similar results. The defects observed in these experiments all exhibit the above feature that the capture rate of the defect is thermally activated. We have found this to be the case using light or current for degradation. This behavior appears to be a universal feature of the MSD. It or similar behavior has been observed in other metastable effects.[2,4] However, the activation energy for production depends on the effect being monitored. Some of the effects studied at low temperature[7] have a low-activation energy. Nevertheless, degradation cannot be activated with the same energy over the entire temperature range above and below room temperature since some of the high-activation energies would predict that degradation would be virtually unobservable at room temperature. We have only been able to measure an activated degradation rate near room temperature when the activation energy is low. More important, the higher the activation energy for annealing, the higher the activation energy for degradation.

The time dependence of solar-cell degradation has been studied in great detail because of important technological implications. The universal behavior is that the degradation varies sublinearly in time with the most common time dependence being $\ln(t)$.[33] Our data, when we monitor photovoltaic properties as in Figs. 14 and 15, are consistent with this. Only at high temperature and for electron trapping have we observed first-order kinetics followed by a saturation in the defect production. For the hole trap MSD the degradation rate varied as $\ln(t)$ even at high temperature.

Although this $\ln(t)$ dependence of the number of trapped charges is not observed in most semiconductors, it has been observed in a-Si:H for gap state trapping by electrons.[34] There is a minimum in the density of states located about 0.5 eV below the conduction-band edge.[24] For trapping by states in this region the number of trapped electrons increases logarithmically with the time that the injecting pulse is applied with no saturation being observed.[24,34] This behavior does not persist in the region of higher density of gap states nor in the vicinity of the dangling bond. In this region first-order kinetics are observed.[24]

To explain the $\ln(t)$ dependence of gap state trapping, I (Ref. 34) postulated that the a-Si:H was microscopically inhomogeneous with electron trapping occurring preferentially in regions distributed randomly throughout the material. These regions become negatively charged reducing further trapping. Clustering of defects is quite likely in a-Si:H because of its nonuniform morphology. It is well known to form a columnar structure during growth,[35] with the size of the columns depending on the growth conditions. We can apply this same defect clustering argument to trapping by the MSD. The density of charge, N_t, trapped on the MSD at a time t would then be[34]

$$N_t = BkT \ln(1 + t/t_0) , \tag{15}$$

where B is a constant proportional to the average charge density. t_0 varies inversely with the capture cross section for the MSD.

A different model to explain the $\ln(t)$ dependence of solar-cell degradation has been proposed by Williams[33] who postulated a distribution of MSD's with different activation energies for production. If the defect production is thermally activated and there is a uniform distribution of activation energies, then an expression for the time dependence of the degradation identical to Eq. (15) results. Thus it does not seem possible to distinguish between the two models from the time dependence of the degradation. In fact any time dependence can be explained by this model by postulating a particular distribution of activation energies. Data presented in Sec. VI show that a distribution of MSD's with different emission energies is likely for some samples.

The data in Fig. 15 show the $\ln(t)$ dependence predicted above. However, the change of the slope ($\mathcal{S}=BkT$) on the $\ln(t)$ plot is much stronger than the linear behavior predicted by Eq. (15). In fact the slope is thermally activated with an activation energy of 0.24 eV, the same as the activation energy for t_0. Thus these models do not seem to be supported by these experiments.

B. Annealing

Most of the measurements described in this article probe the MSD by measuring its annealing kinetics. This permits a determination of the activation energy for emission or annealing of the MSD and its attempt-to-escape frequency. As pointed out in Sec. VI, values of E_e fall into distinct groupings. High values ($E_e > 1.3$ eV) can be associated hole trapping and a low value associated with electron trapping.

Although there has been considerable work on the SW effect and its associated metastable changes in bulk *a*-Si:H and in solar cells, there has been little quantitative work on the annealing dynamics. One usually anneals the MSD at elevated temperature and returns to room temperature for measurements without measuring the associated changes in material parameters as the system returns to equilibrium. This precludes measuring E_e. Jang *et al.*,[2] however, illuminated a variety of phosphorus, boron, or undoped *a*-Si:H at elevated temperatures and then measured the recovery of the dark and photoconductivity at the end of degradation. The thermally activated recovery time separated into two distinct groups: (1) samples (*B* or heavily *P* doped) that showed an *increase* of both dark and photoconductivity after illumination, annealed readily above 100 °C; (2) samples (lightly *P* or undoped) that showed a conductivity *decrease* following illumination, annealed only above 150 °C. The latter change is the classical SW effect.

Arrhenius plots of the relaxation time versus inverse temperature showed that the *increase* in conductivity was associated with a low (0.79–1.00 eV) activation energy whereas the *decrease* in conductivity was associated with a high (1.32–1.53 eV) activation energy. This high activation energy is similar to that originally found for the SW effect.[1,3] Their[2] data can be analyzed to determine ν. We find a spread in ν of $(1-50)\times 10^{+11}$ s^{-1} for the low-activation energy and $(1-20)\times 10^{+14}$ s^{-1} for the high-activation energy data.

A similar low-activation energy for a light-induced conductivity *increase* has been found in compensated *a*-Si:H.[36] The material, which was *P* doped and *B* compensated, has an E_e of 0.55 eV. Analysis of the data gives a ν of 1.5×10^3 s^{-1}. The authors also measured an E_e of 1.55 eV for undoped material that showed the classical conductivity *decrease*. The associated ν is $6\times 10^{+15}$ s^{-1}.

These two groupings of E_e and ν are similar to those found by DLTS. If we assume that the same defects are being produced in both types of measurements then we conclude that the *increase* in conductivity is caused by electron trapping and the *decrease* in conductivity by hole trapping. Since the classical SW effect is a *decrease* in the conductivity it is due to the hole trap MSD. These interpretations are reasonable since we expect the Fermi level to rise when electrons are trapped and to fall when holes are trapped.

C. Models

Since there are now models for the SW effect, we wish to compare our results with the predictions of some of these models. The first concrete model presented[6] and perhaps the most widely accepted is that light breaks weak Si—Si bonds producing dangling bonds. This model stems from the observation that the SW effect is always accompanied by an increase in the characteristic electron paramagnetic resonance of the dangling bond.[6–8] Quantitative measurements[8] of the change in dangling-bond density and photocurrent as a function of light-induced degradation have given additional support to this model.

Because of the symmetry of the activation energies for production and annealing of the electron trap MSD it is best to view it, at least schematically, as a two-level system separated by a high potential barrier, V_b. The potential energy versus configuration coordinate, q, diagram is sketched in Fig. 25. This is a rough diagram. We use only a single coordinate when actually there is a manifold of coordinates or paths that take an electron between the two states. The potential energy minima are not necessarily at the same energy. The state at q_m represents the MSD and its trapped charge. The state at q_0 represents a free charge and annealed defect. One usually assumes that the state q_0 is the ground state. Since *a*-Si:H is amorphous we expect a spectrum of V_b and energy separation, V_s, between the minima. Since the metastable state exists for long times, direct tunneling from q_m to q_0 does not seem likely. Certainly an electron can be thermally activated over the barrier in either direction. Our measurements have shown that the transition, $q_m \rightarrow q_0$, has an activation energy of about 1 eV, with a variation among samples of 0.3 eV. Some samples show a distribution of energy levels. However, most show a single slightly broadened level. The same picture can be used to describe the hole trap MSD. Even though we do not have measurements for the activation energy for production of the hole trap MSD because of the high temperatures required to observe the hole signal, we expect it also to have a high activation energy for production.

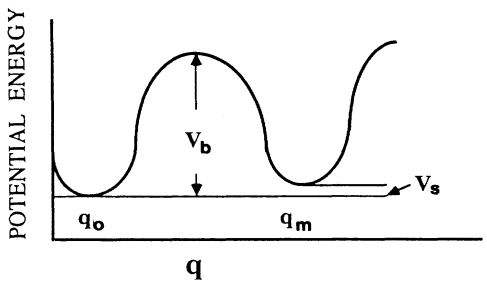

FIG. 25. Configuration coordinate diagram used to schematically describe MSD in *a*-Si:H. The energy minimum at the coordinate q_0 represents the state with a charge located at a band edge and no MSD formed. The state q_m represents the MSD with its associated trapped charge.

The defect production rate is thermally activated irrespective of whether forward bias or light is used to form MSD. In all cases where I could measure the activation energy for production and destruction on the same defect, the activation energy for production was about 10% higher than for annealing. Thus it is appropriate to place the metastable state above the q_0 state. What is surprising is that production is thermally activated with the same energy irrespective of whether light or current is used for degradation. This means that the thermal energy given up by electron-hole recombination is unimportant in affecting the transition over the temperature range where we observe a thermally activated process (400–520 K). This shows that the usual assumption that the MSD must be formed by recombination[8] is not supported by our measurements.

Presumably the reason that others, using light to degrade a sample, have not observed a high activation energy for defect production is because of light-induced annealing. As pointed out by Redfield,[37] a natural consequence of the recombination-induced production model,[8] is recombination-induced annealing. When these two competing processes are dominant, as they are near room temperature, then any temperature effects will reflect the energy difference between the states q_0 and q_m. Only at high temperature, where thermal activation over the barrier dominates these mechanisms, will the true barrier be measured.

It is reasonable that a charge injected into a-Si:H should form a defect. Street[38] pointed out that a-Si:H apparently violates Mott's "8-N" rule[39] with regard to doping. To account for doping in the framework of the "8-N" rule he argued[38] that a dangling bond must be created to permit a phosphorus atom to dope a-Si:H. The equilibrium reaction is

$$P_3{}^0 \rightleftarrows P_4{}^+ + D^- \tag{16}$$

which states that the electron associated with the substitutional $P_4{}^+$ does not go into the conduction band but is trapped to form a negatively charged dangling bond, D^-. Following this he argued that an electron placed in the conduction band would not remain there but would form a dangling bond by the following reversible reaction

$$N_e + \text{Si—Si} \rightleftarrows D^0 + D^- , \tag{17}$$

where N_e is an electron, Si—Si is a silicon—silicon bond, and D^0 is a neutral dangling bond. Because this reaction requires breaking a Si—Si bond there could be a considerable energy barrier separating the two sides of reaction. The law of mass action predicts a linear relation between N_e and D^-. The hole should obey a reaction of the same form as Eq. (17) with a positively charged dangling bond, D^+, being formed. Thus in the presence of light, D^0, D^+, and D^- all will be formed.

Our experiments measure only the trapped charge so that we cannot say whether dangling bonds are formed. It would be of considerable interest to measure both the spin density and trapped charge in the same sample at the same time. Nevertheless, there is considerable evidence for dangling bonds being formed by light or current flow in a-Si:H.[6,8,13,19] Furthermore, measurements[8] have shown that the dangling bond anneals with a spread of activation energies between 0.9 and 1.3 eV. Since this is the same range that we observe it is likely that the electron or hole trap observed by our DLTS measurements is also a dangling bond. With this assumption in mind we can interpret the data in Fig. 16 showing a linear relation between light flux and trapped electrons in accord with the above arguments. If the free-electron density is proportional to the light flux and the trapped charges are D^-, then the data show the linear relation between N_e and D^- predicted by Eq. (17).

Moreover, it is important to realize that the process of forming and annealing the MSD goes in both directions at high temperature and is driven in one direction or the other by the presence or absence of electrons. This was shown by the experiment on an n-type Schottky barrier described in Sec. VI A. If there is an excess of electrons in the sample the MSD is formed. If the electrons are removed (i.e., in the depletion width) the MSD is removed.

It appears that the "8-N" rule[39] predicts that the MSD would be the ground state of the system. In fact this is indeed the situation. The experiment on the Schottky barrier (Fig. 24) demonstrates that if electrons are present in the bulk, then there are more MSD's than when electrons can be removed. Another way of stating this is that in a Schottky barrier there are more MSD's in the bulk than in the depletion width. Thus it is somewhat of a misnomer to refer to the defect as a metastable defect when it actually forms the ground state. However, there is about a 1-eV barrier to reach the ground state. This is the activation energy to produce the MSD.

The defect is metastable only in the sense that it can be annealed if the conditions are changed during annealing from those during production. During annealing, which is usually carried out in the dark, electrons and holes recombine and are not replenished so that the system is driven toward the energy minimum at q_0. If annealing is attempted under illumination the MSD persists. Similarly MSD's formed by charge trapping of one sign can only be annealed if there is an electric field present to remove the charges thermally ejected from the MSD. Otherwise they are retrapped to form MSD's. Measurements[40] on n-type Schottky barriers that have been interpreted as evidence of electronic doping are examples of reducing the equilibrium MSD population by raising the temperature while an electric field is applied. This produces an increase in the conductance because the Fermi level rises when the MSD's are annealed. Of course, the system returns to normal when the field is removed at elevated temperature so that the MSD's can reform. Improvement of solar cells by applying a reverse bias at elevated temperature[41] is another example of bias assisted annealing.

Because of the symmetry involved in production and annealing of the MSD, we feel that it is a native defect consisting of a neighboring dangling-bond pair of the form D^0D^+ or D^0D^- that has undergone reorientation to produce a barrier against recombination to form a Si—Si bond. This model does not require the presence of hydrogen. However, it could well be that there is a weak bond where H has passivated a native D^0. Also the presence of H at the dangling-bond pair could help

to stabilize them.[8] The fact that only a limited number of MSD's can be formed under intense illumination is consistent with there being a limited number of possible Si—Si bonds available for MSD formation. However, this could also be explained by light-induced annealing.

At low temperature it is possible that electron-hole recombination might play a significant role in defect formation because extrapolation of the high-temperature production rate would indicate a vanishingly small defect production rate at room temperature. We have made crude estimates of the capture cross section for the process at infinite temperature from the amount of absorbed light and the activation energy. We find that the number of defects produced per absorbed photon is between 10^{-2} and 10^{-4}. For an activation energy of 1 eV this translates into a defect production probability of 10^{-19} to 10^{-21} at room temperature. This is considerably lower than the dangling-bond production probability of on the order of 10^{-10} at room temperature.[8] Thus it is more than likely that some other process such as electron-hole recombination[8] or tunneling becomes important near room temperature.

VIII. SUMMARY

We have shown how a systematic study using capacitance and photovoltaic transient DLTS measurements on *p-i-n*, *n-i-p*, and Schottky-barrier devices can be used to determine fundamental properties of light- or current-induced defects, MSD's. Methods of applying capacitance measurements to probe properties of defects in the *i* layer of *p-i-n* and *n-i-p* devices have been described. By making measurements over a wide temperature range, the annealing as well as the production of MSD's could be studied in detail. Measurements on a variety of devices using both current and light to form the MSD's have yielded the properties of the MSD's summarized below.

(1) It is only necessary to inject a single charge to form a MSD by charge trapping. Both positively and negatively charged MSD's (MSD^+ and MSD^-, respectively) can be formed in the same sample provided both signs of charge are injected. Light absorption as well as double injection produce both signs of MSD's.

(2) There is a potential barrier for MSD production. It is about 1 eV for MSD^- and higher for MSD^+. Near room-temperature tunneling or thermal energy supplied by electron-hole recombination can overcome this barrier.

(3) The main activation energy for annealing an MSD^- is about 1 eV. In some samples a distribution of activation energies is observed. In samples with *C* or *F*, the apparent activation energy for the MSD^- is as low as 0.4 eV. Concomitant with the low-activation energy is a low attempt-to-escape frequency.

(4) At elevated temperature, production of MSD^- by light obeys first-order kinetics with all of the potential defects being produced with strong illumination. The number of MSD^+'s produced increases sublinearly with time with no indication that all the possible MSD^+'s can be formed.

(5) The sign of the MSD can be correlated with different effects. The MSD^+ produces the SW effect. The MSD^- is responsible for an increase in conductivity. Both MSD^+ and MSD^-, however, cause solar-cell degradation.

(6) The data are consistent with the MSD being associated with dangling-bond formation so that the MSD^+ can be identified as a D^+ and the MSD^- as a D^- dangling bond. However, it is likely that a D^0 is formed along with each charged defect.

[1]D. L. Staebler and C. R. Wronski, Appl. Phys. Lett. **31**, 292 (1977).

[2]J. Jang and C. Lee, J. Appl. Phys. **54**, 3934 (1983); J. Jang, T. M. Kim, and J. K. Hyun, J. Non-Cryst. Solids, **59&60**, H29 (1983).

[3]D. L. Staebler and C. R. Wronski, J. Appl. Phys. **51**, 3262 (1980).

[4]J. Pankove and J. E. Berkeyheiser, Appl. Phys. Lett. **38**, 456 (1980); K. Morigaki, I. Hirabayashi, and M. Nitta, Solid State Commun. **33**, 851 (1980).

[5]H. Schade and J. I. Pankove, J. Phys. (Paris), Colloq. **42**, C4-327 (1981).

[6]H. Dersch, J. Stuke, and J. Beichler, Appl. Phys. Lett. **38**, 456 (1980).

[7]I. Hirabayashi, K. Morigaki, and S. Nitta, Jpn. J. Appl. Phys. **19**, L357 (1980).

[8]M. Stutzmann, W. B. Jackson, and C. C. Tsai, Appl. Phys. Lett. **45**, 1075 (1984); Phys. Rev. B **32**, 23 (1985).

[9]D. V. Lang, J. D. Cohen, J. P. Harbison, and A. M. Sergent, Appl. Phys. Lett. **40**, 474 (1980); J. D. Cohen, D. V. Lang, J. P. Harbison, and A. M. Sergent, Sol. Cells **9**, 119 (1983).

[10]J. Stoica, J. Phys. (Paris), Colloq. **42**, C4-407 (1981).

[11]M. Grunwald, K. Weber, W. Fuhs, and P. Thomas, J. Phys. (Paris), Colloq. **42**, C4-523 (1981).

[12]J. Beichler, H. Mell, and K. Weber, J. Non-Cryst. Solids, **59&60**, 257 (1983); C. Y. Huang, S. Guha, and S. J. Hudgens, Phys. Rev. B **27**, 7460 (1983).

[13]N. Amer, A. Skumanich, and W. B. Jackson, Physica B&C **117-118**, 897 (1983).

[14]D. L. Staebler, R. S. Crandall, and R. Williams, Appl. Phys. Lett. **39**, 733 (1981).

[15]R. S. Crandall, Phys. Rev. B **24**, 7457 (1981).

[16]R. S. Crandall and D. L. Staebler, Sol. Cells **9**, 63 (1983).

[17]R. S. Crandall, D. E. Carlson, A. Catalano, and H. A. Weakliem, Appl. Phys. Lett. **44**, 200 (1984).

[18]See, Sol. Cells **9** (1983) for reports on, Proceedings of a SERI Workshop on Light Induced Changes, San Diego, California, 1982 (unpublished).

[19]H. Yamagishi, H. Kida, T. Kanada, H. Okamoto, and Y. Hamakawa, Appl. Phys. Lett. **47**, 860 (1985).

[20]R. S. Crandall, in *Tetrahedrally-Bonded Amorphous Semiconductors,* edited by David Adler and Helmut Fritzsche (Plenum, New York, 1985).

[21]D. V. Lang, in *Thermally Stimulated Relaxation in Solids,* Vol. 37 of *Topics in Applied Physics,* edited by P. Braunlich (Springer, Berlin, 1979), p. 93.

[22]J. D. Cohen and D. V. Lang, Phys. Rev. B **25**, 5350 (1982).
[23]D. E. Carlson, Sol. Energy Mat. **3**, 503 (1980).
[24]J. D. Cohen, in *Hydrogenated Amorphous Silicon, Part C,* Vol. 21 of *Semiconductors and Semimetals,* edited by R. K. Willardson and A. C. Beer (Academic, New York, 1984).
[25]A. R. Moore, J. Appl. Phys. **54**, 322 (1983).
[26]R. S. Crandall, RCA Rev. **42**, 441 (1981).
[27]S. M. Sze, *Physics of Semiconductor Devices,* 2nd ed. (Wiley-Interscience, New York, 1963), p. 94.
[28]R. S. Crandall, J. Appl. Phys. **53**, 3350 (1982); **55**, 4418 (1984).
[29]S. Guha, J. Yang, W. Czubatyj, S. J. Hudgens, and M. Hack, Appl. Phys. Lett. **42**, 588 (1983).
[30]A. Skumanich, N. M. Amer, and W. B. Jackson, Phys. Rev. B **31**, 2253 (1985).
[31]R. S. Crandall, J. Appl. Phys. **54**, 7176 (1983); B. W. Faughnan and R. S. Crandall, Appl. Phys. Lett. **44**, 537 (1984).
[32]R. A. Street, J. Kakalios, and T. M. Hayes, Phys. Rev. B **34**, 3030 (1986).
[33]R. Williams, Inner Mongolia Electronics (in Chinese) **5**, 1 (1984).
[34]R. S. Crandall, J. Electron. Mater. **9**, 713 (1980).
[35]J. C. Knights, G. Lucovsky, and R. J. Nemanich, J. Non-Cryst. Solids **32**, 393 (1979).
[36]H. Mell and W. Beyer, J. Non-Cryst. Solids **59&60**, 405 (1983).
[37]D. Redfield, Appl. Phys. Lett. **48**, 846 (1986).
[38]R. A. Street, Phys. Rev. Lett. **49**, 1187 (1982).
[39]N. F. Mott, Adv. Phys. **16**, 49 (1967).
[40]D. V. Lang, J. D. Cohen, and J. P. Harbison, Phys. Rev. Lett. **48**, 421 (1982).
[41]G. Swartz, Appl. Phys. Lett. **44**, 697 (1984).